Asian Journal of Current Research in Clinical Cancer
ISSN: 3062-4444
2024, Volume 4, Issue 1, Page No: 142-163

Available online at: www.galaxypub.co/page/journals

Galaxy Publication

Galaxy Publication

A Membrane-Proximal CD19–Targeted CAR T Cell With Rapid Binding Kinetics Overcomes Resistance In Relapsed B-Cell Lymphoma

Daniel I. Ferrari[1], Ingrid K. Alvarez[1], Maria Zhang[1], Lina Wilson[1], Rebecca Y. Ramirez[1]*

[1]Department of Cancer Biology, Faculty of Medicine, University of Zurich, Zurich, Switzerland.

***E-mail** ✉ rramirez@hotmail.com

Received: 23 May 2024; **Revised:** 15 August 2024; **Accepted:** 16 August 2024

ABSTRACT

Approved anti-CD19 chimeric antigen receptor T-cell treatments (CART19) demonstrate effectiveness in treating advanced B-cell non-Hodgkin lymphoma (NHL), although relapse occurs in the majority of cases. Multiple factors drive treatment failure, including emergence of CD19-negative disease and impaired CAR T-cell activity. Each of the four licensed CART19 therapies relies on the FMC63 single-chain variable fragment (scFv), which binds a membrane-distal CD19 epitope with slow binding (on) and release (off) kinetics. We postulated that an innovative anti-CD19 scFv directed at a distinct membrane-proximal CD19 epitope—unrelated to the FMC63 binding site—and exhibiting rapid on- and off-rates might reduce instances of CART19 failure and enhance therapeutic outcomes. An autologous CART19 therapy incorporating 4-1BB costimulation was engineered using a new humanized avian-derived antibody (h1218). This antibody recognizes a membrane-proximal CD19 epitope and shows quicker on/off kinetics relative to FMC63. Performance of h1218-CART19 was evaluated in vitro and in vivo against models refractory to FMC63-CART19. A multicenter first-in-human phase I trial was initiated to assess AT101 (GMP-grade h1218-CART19) in individuals with relapsed/refractory (r/r) NHL. In preclinical studies, h1218-CART19 alone—unlike FMC63-CART19—successfully eliminated lymphomas bearing CD19 point mutations (L174V and R163L) or those co-expressing FMC63-CAR19, as observed in relapses following FMC63-CART19 therapy. Moreover, h1218-CART19 displayed superior cytotoxicity against B-cell tumors both in vitro and in vivo versus FMC63-CART19. At the mechanistic level, h1218-CART19 demonstrated lower activation-induced cell death (AICD) and superior proliferation relative to FMC63-CART19, attributable to its rapid on- and off-rates. Guided by these findings, a phase I dose-escalation study was conducted, evaluating three dose levels (DL) of AT101 (GMP h1218 product) in a 3 + 3 scheme. Across 12 enrolled patients (7 DLBCL, 3 FL, 1 MCL, and 1 MZL), AT101 exhibited an acceptable safety profile, including 8.3% grade 3 CRS (n = 1) and 8.3% grade 4 ICANS (n = 1). Overall response rate reached 91.7% with a complete response rate of 75.0%, rising to 100% at DL-2 and -3. Peak AT101 levels correlated with complete response and B-cell depletion. An innovative, well-tolerated, and highly active CART19 therapy has been created that targets a membrane-proximal CD19 region with rapid binding and release kinetics, delivering robust activity and favorable safety in relapsed B-cell NHL cases.

Keywords: CD19, CAR T cells, Resistance, CD19 mutations, Epitope masking, Lymphoma

How to Cite This Article: Ferrari DI, Alvarez IK, Maria Zhang M, Wilson L, Ramirez. RY. A membrane-proximal CD19–targeted CAR T cell with rapid binding kinetics overcomes resistance in relapsed B-cell lymphoma. Asian J Curr Res Clin Cancer. 2024;4(1):142-63. https://doi.org/10.51847/7dHofGlL67

Introduction

Therapies using CD19-targeted chimeric antigen receptor T cells (CART19) have achieved remarkable results in CD19-positive B-cell cancers. Nevertheless, numerous patients fail to attain complete response (CR) or suffer subsequent relapse after CART19, with varying relapse frequencies across disease entities [1]. The strength and quality of CAR-CD19 binding on malignant cells play a pivotal role in determining CAR T-cell efficacy. All currently FDA-approved CART19 agents—tisagenlecleucel, lisocabtagene maraleucel, axicabtagene ciloleucel, and brexucabtagene autoleucel—incorporate single-chain variable fragments (scFv) based on the murine FMC63 anti-human CD19 antibody [2-4]. The FMC63 binding site on CD19 spans exons 2 through 4 [5]. Notably, certain

relapse pathways involve disappearance of the FMC63-bound CD19 epitope via point mutations or epitope concealment [6-8]; additionally, suboptimal CAR:CD19 engagement may impair CAR T-cell performance [9-11].

Surface CD19 expression may persist in relapsed tumors, yet the FMC63 epitope becomes inaccessible to CART19 due to diverse processes. Such FMC63 epitope absence encompasses direct mutation within the epitope [12] or concealment by the CAR19 molecule itself [13]. Multiple CD19 point mutations have emerged in diffuse large B-cell lymphoma (DLBCL) and B-acute lymphoblastic leukemia (B-ALL) cases resistant to CART19, with some alterations disrupting FMC63 recognition and causing FMC63-CART19 ineffectiveness [8, 12, 14]. Furthermore, our prior work uncovered a unique resistance pathway wherein the CAR19 transgene inadvertently transduced malignant B-cells during production, enabling cis CAR19:CD19 binding that conceals the epitope and fosters resistance [13]. Thus, engaging CD19 sites distinct from FMC63 could circumvent epitope loss induced by FMC63-CART19.

Furthermore, suboptimal T-cell activity represents an additional key factor in FMC63-CART19 treatment failure. Numerous contributors drive this problem, including inherent T-cell traits (like differentiation or exhaustion levels) and the hostile tumor microenvironment, yet the characteristics of the CAR-CD19 synapse remain essential for optimal CAR T immunotherapy outcomes [15]. As an illustration, prior work has revealed that engaging a membrane-proximal CD22 epitope facilitates superior immune synapse assembly and markedly better in vivo antitumor efficacy compared to a distal epitope [16, 17]. Similarly, structural modifications to the CAR—such as reducing the hinge length connecting the scFv variable domains—have been shown by us and others to enhance target access by bringing CAR T cells closer to malignant cells, thereby amplifying effector capabilities [18]. The kinetics of CAR-target binding and release also profoundly affect CAR T-cell behavior. Theory and data indicate that CAR designs allowing quicker detachment from targets promote longer-lasting functional persistence [11, 19].

In order to overcome relapse after FMC63-CART19, we put forward two hypotheses: 1. a CART19 construct recognizing a CD19 site unrelated to the FMC63 epitope and positioned nearer the cell surface would evade epitope loss while augmenting T-cell performance; and 2. rapid binding and dissociation kinetics would diminish activation-induced T-cell death (AICD) and exhaustion. Accordingly, we designed a novel humanized antibody (h1218) that binds a membrane-proximal CD19 region spanning amino acids 51–63 (within exon 2) and possesses accelerated on- and off-rates. We then built a second-generation CAR incorporating this h1218 scFv together with 4-1BB and CD3ζ signaling modules. After rigorous functional benchmarking of h1218-CART19 versus standard FMC63-CART19 in preclinical systems, and with robust supportive data, we progressed the h1218-based product (designated AT101) into a multicenter, first-in-human phase I study enrolling patients with relapsed/refractory non-Hodgkin lymphomas. Results from this study indicated substantial complete remission rates accompanied by acceptable toxicity.

Materials and Methods

Anti-CD19 scFv discovery and affinity maturation

To identify a novel antibody against the human CD19 extracellular domain (ECD) distinct from FMC63, we executed competitive biopanning using a pre-formed complex of recombinant human CD19 ECD (M1-P278) bound to FMC63 scFv to shield the FMC63 site. Screening employed a proprietary immunized chicken antibody library (Patent US16/768412) derived from avian immunization with human CD19. Initial hits were detected via periplasmic extract assays and confirmed by cell-based ELISA using CD19-expressing (Raji) versus non-expressing (K562) lines. Promising candidates were reformatted as scFv with a (G4S)3 linker, expressed in HEK293F cells, and affinity-purified using a C-terminal human Fc tag. Antibody 1218 was chosen as the lead for its selective engagement of a non-FMC63 CD19 site. Affinity enhancement involved randomizing six CDR positions in heavy and light chains via NNK codons while preserving ≥70% parental sequence identity. Improved variants were isolated by Raji cell-binding EC50 criteria. The matured 1218 variant carried three substitutions in light-chain CDR3 and achieved >10-fold better EC50 versus the original. For clinical suitability, the avian 1218 scFv underwent humanization by CDR grafting onto selected human germline frameworks identified through IMGT/V-QUEST: heavy chain utilized IGHV3-21*04 and IGHJ5*01; light chain used IGLV1-51*02 and IGLJ2*01. The completed h1218 scFv—encompassing humanized light variable domain, (G4S)3 linker, and

humanized heavy variable domain—was gene-synthesized by GenScript (Jiangsu, China) and produced in HEK293F cells.

Epitope binning assay

Competitive epitope mapping of h1218 was conducted on an 8-channel Octet platform (Octet QKe, Pall ForteBio). AR2G biosensors (Amine Reactive 2nd Generation, Pall ForteBio; Cat# 18–5092) were functionalized with 10 μg/mL FMC63 Fc followed by capture of 10 μg/mL CD19 ECD-kappa light chain fusion (CD19-ECD-Ck) for 10 min. After baseline stabilization, sensors were exposed to 10 μg/mL of either FMC63 or h1218 for 10 min to probe for incremental binding. Absorbance at 450 nm was quantified on an ELISA plate reader (Victor X3, PerkinElmer).

Construction of CD19 variant cell lines and epitope mapping via mutagenesis

Mutant human CD19-T2A-GFP and cynomolgus CD19-T2A-GFP constructs (Bioneer, Daejeon, Korea) were inserted into pLenti6.3 vector (Invitrogen; Cat# K5315-20). Domain-swapped chimeric CD19 molecules were assembled by overlap extension PCR and cloned into pLenti6.3 using the parental human and cynomolgus templates. Single-point CD19 mutants were similarly generated via overlap extension PCR targeting critical residues. Lentivirus encoding wild-type (WT), chimeric, or point-mutant CD19 was packaged in LentiX 293T cells. Target cell lines were transduced and selected with blasticidin (Invitrogen; Cat# R210-01). Antibody reactivity against HEK293T cells expressing each CD19 variant was quantified by flow cytometry via mean fluorescence intensity (MFI).

Affinity measurement assay

The binding strengths of h1218 and FMC63 single-chain variable fragments (scFvs) were assessed with the Octet biosensor platform. In short, the purified scFvs were attached to an AR2G sensor chip (Amine Reactive 2nd Generation, Pall ForteBio; Cat# 18–5092) through routine amine coupling procedures. Recombinant human CD19 extracellular domain with a Cκ tag (M1-P278) was passed over the sensor surface at a steady flow rate, using concentrations of 12.5–400 nM for h1218 scFv and 50–1600 nM for FMC63. The binding (association rate) and release (dissociation rate) kinetics were tracked via OD450 measurements, and results were analyzed with a 1:1 binding model.

Off-Target scFv binding analysis: retrogenix assay

To evaluate potential off-target binding of the CARs, both h1218 and FMC63 scFvs were tagged with fluorescence and tested against fixed HEK293 cells/slides expressing 5,484 different vectors. Each vector co-expressed ZsGreen1 alongside either a full-length human plasma membrane protein or a tethered human secreted protein, with all tests run in duplicate (16 slide sets, n = 2 slides per slide set). Fluorescence imaging (Alexa Fluor 647 and ZsGreen1 channels) was analyzed with ImageQuant software, revealing 16 initial positive hits (appearing as duplicate spots). These hits showed varying signal strengths relative to background, from faint to intense. For validation, fresh slides containing all 16 hits were treated with h1218 scFv protein in duplicate. All screening, validation, and data processing steps were carried out by Retrogenix, part of Charles River Laboratories.

Generation of the CAR construct and preclinical lentiviral vector production

The conventional FMC63-CAR (known as CTL019) is composed of the FMC63 scFv linked to 4-1BB and CD3ζ signaling domains [20]. Similarly, the h1218-CAR was built using the h1218 scFv with the same 4-1BB and CD3ζ components. Both CARs were inserted into replication-incompetent, third-generation lentiviral vectors (pTRPE or pLTG). In brief, each T175 flask was seeded with 8×10^6 HEK293T cells in RPMI 1640 medium (Gibco; Cat# 11875–085) containing 10% fetal bovine serum (FBS, Gibco; Cat# 16140–071), followed by overnight incubation at 37 °C. At 24 h, when cells were ~ 70–80% confluent, transfection was done using Lipofectamine 2000 (116 μL, Invitrogen), up to 18 μg of each packaging plasmid, and 15 μg of CAR plasmid per flask. The transfection reagents and DNA were first diluted in 4.6 mL Opti-MEM Reduced Serum medium (ThermoFisher) before adding to the flasks. Media were harvested at 24 h and 48 h after transfection, passed through 0.45 μm filters, and concentrated via ultracentrifugation (8,000 × g for 16–18 h or 25,000 × g for 2.5 h). Viral titers were measured in HEK293T cells, and CAR expression was confirmed by flow cytometry using specific antibodies.

Preclinical CAR T cell production

CAR T cells were manufactured following an established protocol [21]. Normal human primary T cells were provided by the Human Immunology Core at the University of Pennsylvania. Equal numbers of CD4 and CD8 T cells (1:1 ratio) were stimulated in culture with CD3/CD28 Dynabeads (Gibco; Cat# 40203D) at a 3:1 bead-to-cell ratio for 6 days. On day 2 of stimulation, lentivirus was introduced at a multiplicity of infection (MOI) of 1.5. Starting from day 6 (after bead removal), cell numbers and volumes were monitored every two days with a Multisizer 3 Coulter Counter (Beckman). Once cell expansion slowed, size stabilized, and volume approached ~ 350 fL, the CAR T cells were cryopreserved in 90% FBS plus 10% DMSO. For any downstream experiments, cells were thawed and recovered overnight at 37 °C in RPMI with 10% FBS.

Cell Lines and general cell culture

The B-cell lymphoma lines used (Raji, Nalm6, OCI-Ly18, Toledo, and Pfeiffer) were sourced originally from ATCC or DSMZ. The LentiX 293 T line came from Takara Bio. Every cell line underwent short tandem repeat (STR) profiling for identity confirmation (University of Arizona) and was checked for mycoplasma every two months (Lonza; Cat# LT07-710). Cultures were grown in R10 medium—RPMI 1640 base with 10% FBS, 1% GlutaMAX (Gibco; Cat# 35050–079), 1% Pen/Strep (Gibco; 15140–122), and 1% HEPES (Gibco; Cat# 15630–130)—at 37 °C under 5% CO_2.

Flow cytometry

Samples from in vitro or in vivo studies were incubated with fluorescent antibodies for 15 min in the dark, then washed once in PBS (Gibco; Cat# 10010031) with 2% FBS. Absolute counts of cells (such as tumor or T cells) were obtained by adding Flow-Count Fluorospheres (Beckman Coulter; Cat# 754053) as per the instructions. Apoptosis was measured with CellEvent Caspase3/7 Green Flow Cytometry Assay (Invitrogen; Cat# C10427) following the provided protocol. Gating began with forward and side scatter to select cells of interest, then singlets, and finally live cells using ViaKrome 808 fixable viability dye (Beckman Coulter; Cat# C36628). FMC63-CAR19 surface levels were detected with a PE-conjugated anti-idiotype antibody (Novartis). Acquisitions were run on a 6-laser Cytoflex LS instrument (Beckman Coulter), and all files were analyzed in FlowJo version 9.0 or 10 (FlowJo, LLC, BD).

Cytotoxicity assays

Target cells were modified with a lentiviral vector encoding Click Beetle Green luciferase (CBGLuc) fused to GFP and then purified via sorting on a FACS Melody Cell Sorter (BD). In brief cytotoxicity tests, target cells were co-incubated with CAR T cells or appropriate controls at the specified effector-to-target (E:T) ratios, adhering to the recommended protocol. D-luciferin potassium salt (Gold Biotechnology; Cat# 115144–35-9) was dissolved in PBS to reach 15 mg/mL and added to the co-cultures, followed by a 10-min incubation at 37 °C. Viable cell numbers were determined by capturing bioluminescence signals on a BioTek Synergy H4 reader, with processing handled by BioTek Gen5 software (Agilent Technologies). The percentage of target-specific killing was computed based on signals from target cells alone, without effectors.

In prolonged killing experiments, CAR T cells were mixed with malignant target cells at E:T ratios of 0.125:1 or 0.0625:1. Every 48–72 h, absolute quantities of both T cells and tumor cells were assessed by flow cytometry incorporating CountBright absolute counting beads (ThermoFisher; Cat# C36950). Cell densities in the co-cultures were consistently adjusted to 1×10^6 cells/mL.

Cytokine secretion assay

Effector and target populations were co-cultured at 5:1 or 3:1 ratios in R10 medium for 24 h. Supernatants were harvested and, if not analyzed immediately, stored at -80 °C. Quantification of released cytokines was carried out with ELISA MAX kits for human IL-2 (BioLegend; Cat# 431801) or human IFN-γ (BioLegend; Cat# 430101 and BD Biosciences; Cat# 555142).

Cell avidity measurement using z-movi

The interaction strength between CAR T cells and a Nalm6 cell monolayer was quantified on a z-Movi Cell Avidity Analyzer (LUMICKS). Acoustofluidic chips designed for z-Movi were first treated with poly-L-lysine (Sigma-Aldrich; Cat# P4707) for 3 h to promote adhesion. Each chip received 2×10^6 Nalm6 cells suspended at

1×10^8 cells/mL, which were allowed to settle and attach during a 2-h incubation at 37 °C in a non-humidified incubator. Subsequently, 1×10^5 CAR T cells (pre-stained with CellTracker Deep Red Dye; ThermoFisher; Cat# C34565) were layered onto the monolayer and permitted to bind for 15 min. Detachment was induced by applying acoustic waves, and the process was recorded for analysis in ImageJ and R. All avidity measurements followed the protocols and suggestions provided by the manufacturer (LUMICKS), with final avidity scores calculated via z-Movi software (v1.0).

Xenograft mouse models

NSG mice (NOD.Cg-Prkdcscid Il2rgtm1Wjl/SzJ), 6–8 weeks old, were sourced from the Stem Cell and Xenograft Core at the University of Pennsylvania and kept in specific pathogen-free housing. The tumor lines (Raji and Nalm6) were transduced to express CBGLuc for imaging. Leukemia was established by tail-vein injection of 1×10^6 Nalm6 cells suspended in 0.15 mL sterile PBS. Disease progression was followed non-invasively with a Xenogen IVIS system (PerkinElmer), recording bioluminescence intensity (BLI) 10 min after injecting luciferin (100 mg/kg; GoldBio; Cat# LUCK-1G). Once BLI averaged ~10^7 total flux (P/S), usually 5–7 days after tumor inoculation, mice were treated intravenously with the planned number of CAR-expressing T cells or control untransduced T cells (UTD). Mice were regularly checked for signs of tumor advancement or treatment-related adverse effects, including xenogeneic graft-versus-host disease markers like >10% weight reduction, rough coat, diarrhea, eye inflammation, or paralysis of rear limbs. Animal husbandry and experiments complied with NIH Guidelines, and all studies were reviewed and approved by the University of Pennsylvania Institutional Animal Care and Use Committee (IACUC).

Confocal microscopy imaging of the immune synapse

Planar supported lipid bilayers were created by depositing and fusing liposome vesicles onto cleaned glass coverslips, following prior methods [22]. Liposomes were confined within a μ-Slide VI 0.4 flow chamber (Ibidi; Cat# 80606). Bilayers underwent blocking with 5% casein for 20 min, then exposure to 6.3 nM streptavidin (ThermoFisher; Cat# 434301) for 15 min. Following buffer washes (HEPES-buffered saline), Alexa Fluor 647-conjugated biotinylated CD19 antigen (R&D Systems; Cat# AVI9269) was added for 30 min at room temperature. Remaining streptavidin sites were capped with 2.5 μM D-biotin. CAR T cells were placed on these antigen-presenting bilayers and activated for 2 h at 37 °C. Fixation was performed with 4% paraformaldehyde for 15 min, followed by permeabilization using 0.5% Triton-X100 in PBS with 10% normal donkey serum for 30 min at room temperature. Intracellular staining employed antibodies specific for perforin (dG9, BioLegend; Cat# 308105), phosphorylated CD3ζ (Y83, Abcam; Cat# ab68236), and phosphorylated ZAP70 (Tyr318, Cell Signaling; Cat# 2701), as reported earlier [23]. Polymerized actin was highlighted with Alexa Fluor 405-phalloidin (ThermoFisher; Cat# A30104). High-resolution images were acquired on a Nikon A1R HD confocal system.

General preclinical work statistical analysis

In vitro results shown are from a minimum of two independent replicates. Values are displayed either as single data points or mean ± standard error of the mean (SEM). Pairwise group differences were tested with an unpaired two-tailed Student's t-test. For analyses involving three or more groups, one-way ANOVA was used, applying Tukey's multiple comparison correction unless stated differently. Kaplan-Meier survival estimates were compared via the log-rank (Mantel-Cox) test. Significance levels are marked as: * $p < 0.05$, $p < 0.01$, * $p < 0.001$, $p < 0.0001$. All computations were done in GraphPad Prism version 9.0 (San Diego, CA).

Study protocol overview

A phase I, multicenter, open-label, non-randomized trial was performed across two sites in South Korea, utilizing a 3 + 3 dose-escalation scheme. Details regarding eligibility criteria are provided in the primary manuscript. Following apheresis and production of chimeric antigen receptor (CAR) T cells, participants underwent a conditioning regimen involving intravenous administration of fludarabine (25 mg/m² on days -4 through -2) and cyclophosphamide (250 mg/m² on days -4 through -2). This conditioning protocol mirrored the one authorized by the FDA for the CD19-directed CAR T product tisagenlecleucel [24]. To mitigate potential reactions, patients received acetaminophen and diphenhydramine 30–60 minutes prior to infusion of the CAR T product. The CAR T cells were delivered in a single infusion at one of three escalating dose cohorts. Due to the investigational status of this first-in-human investigation, both conditioning chemotherapy and cell infusion occurred in a hospital

setting. The cohorts were defined as follows: DL-1 at 0.2×10^6 cells/kg, DL-2 at 1.0×10^6 cells/kg, and DL-3 at 5.0×10^6 cells/kg. Efficacy evaluations were scheduled for months 1, 3, 6, and 12 post-infusion, or more frequently if clinically warranted. Extended monitoring was intended annually for a period of five years. Primary objectives focused on assessing the safety profile and production success rate of the CAR T cells. Secondary objectives encompassed treatment response rates, duration of CAR T cell detection in vivo, rates and length of B-cell depletion and low gamma globulin levels, as well as progression-free survival (PFS) and overall survival (OS) rates at the one- and two-year marks. Regulatory oversight was provided by Korea's Ministry of Food and Drug Safety (MFDS) along with institutional review boards at each site. The trial is listed on ClinicalTrials.gov under identifier NCT05338931. Sponsorship was provided by AbClon Inc. All enrolled individuals supplied written informed consent compliant with the Declaration of Helsinki prior to participation. Data included in this analysis pertain to all individuals treated with AT101 up to December 19, 2022, with the most recent follow-up date being September 25, 2023.

Production of clinical-grade AT101 CAR T cells

This phase I investigation of AT101 adhered to guidelines set forth by the Ministry of Food and Drug Safety (MFDS), the national regulatory authority in South Korea. Manufacturing of GMP-grade AT101 employed the fully automated, closed-platform CliniMACS Prodigy system (Miltenyi). Starting material from apheresis was introduced into the Prodigy device via the TS520 tubing set, followed by positive selection of CD4+ and CD8+ T lymphocytes using CliniMACS reagents. An initial load of 5×10^7 CD3+ T cells was placed in the system for activation via CD3/CD28 beads (TransAct, Miltenyi) supplemented with recombinant human IL-2 (MACS GMP, Miltenyi). On culture day 1, cells underwent transduction with GMP-grade h1218 lentiviral vector (Lentigen) at a multiplicity of infection of 1, with expansion continued until reaching up to 4×10^9 cells. Per MFDS requirements, product release criteria incorporated culture-based assays for replication-competent lentivirus (RCL), adventitious agents, and microbial sterility.

Evaluation of toxicity and treatment response

Grading of cytokine-release syndrome (CRS) and immune effector cell-associated neurotoxicity syndrome (ICANS) followed the consensus criteria from the American Society for Transplantation and Cellular Therapy [25]. All other adverse effects were classified using the Common Terminology Criteria for Adverse Events, version 5.0. Imaging studies (PET-CT, CT, or MRI) in patients with lymphoma receiving AT101 were interpreted based on the Lugano response criteria [26].

Statistical considerations

Continuous data are reported as medians accompanied by ranges (unless noted otherwise), while categorical data are expressed as proportions. Progression-free survival represents the interval from AT101 administration to documented disease progression, death, or censoring at the latest assessment. Overall survival spans from the infusion date to death or last known alive date. All statistical computations and graphical representations were generated with GraphPad Prism version 9.5.0 (730). As the primary goal of this early-phase trial was identification of the maximum tolerated dose (MTD) and selection of a recommended phase II dose (RP2D) through evaluation of safety and tolerability, formal hypothesis testing was not applied.

Results and Discussion

Discovery of h1218, a novel humanized avian scFv targeting a membrane-proximal epitope on human CD19

Our initial objective was to develop an antibody directed against a CD19 epitope different from the one bound by the FMC63 antibody, which is incorporated in all currently FDA-approved CD19-targeted CAR T therapies **(Figure 1a).** To achieve this, we interrogated a proprietary chicken-derived immune single-chain variable fragment (scFv) library using the extracellular domain of human CD19 (M1-K291). The larger phylogenetic distance between chickens and humans, relative to mice and humans, facilitates the isolation of antibodies against epitopes not typically accessed by murine sources. Primary screening yielded six candidates, among which clone 1218 was chosen due to its lack of competition with FMC63 for binding to CD19 (M1-P278). Epitope binning via Octet biosensor analysis demonstrated simultaneous binding of FMC63 and h1218 to CD19 **(Figure 1b),** verifying recognition of separate epitopes. The avian 1218 scFv was subsequently humanized through CDR grafting onto

human germline frameworks with selected backmutations, resulting in the humanized h1218 scFv. To map the epitope bound by the 1218 scFv, we conducted domain-swapping and mutagenesis studies. The CD19 extracellular region was segmented into three domains, and each human (H) domain was substituted with the corresponding cynomolgus (C) monkey sequence, producing chimeras: H–H-H-(cell), C-H–H-(cell), H-C-H-(cell), and H–H-C-(cell). Binding of h1218 scFv was preserved with H–H-C but abolished with C-H–H, indicating that—unlike FMC63—the h1218 scFv targets an epitope within the membrane-proximal domain spanning amino acids 51 to 63 **(Figure 1c).** Fine-mapping through single-residue substitutions identified L58, K59, and K63 as critical for h1218 binding. In contrast, the membrane-distal residue H218/KSS [27] was essential for FMC63 recognition **(Figure 1d).** ELISA-based assessment of interferon-gamma secretion by h1218-CAR T cells confirmed marked reduction upon mutation of L58, K59, or K63, with milder effects from changes at T51, S53, and E55 **(Figure 1e).** Affinity measurements revealed comparable equilibrium dissociation constants for h1218 and FMC63 scFvs against CD19-ECD-Ck (mean KD: 1.85×10^{-7} M and 1.49×10^{-7} M, respectively), although kinetic profiles differed substantially **(Figure 1f).** Notably, h1218 exhibited a faster association rate (mean Kon: FMC63 = 8.94×10^{3} (1/Ms) versus h1218 = 8.68×10^{4} (1/Ms)) and a slower dissociation rate (mean Koff: FMC63 = 1.31×10^{-3} (1/s) versus h1218 = 1.60×10^{-4} (1/s)).

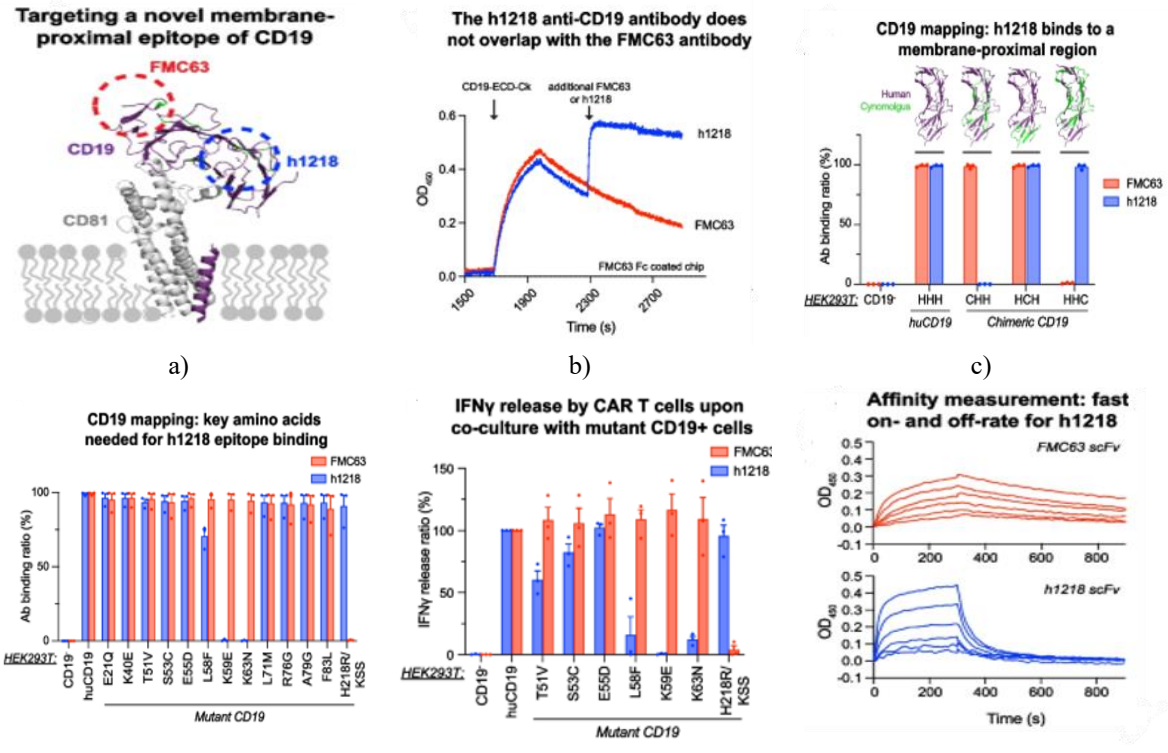

Figure 1. The h1218 antibody displays specificity for CD19 and binds a membrane-proximal epitope distinct from FMC63. a) Diagram illustrating binding locations of FMC63 and h1218 on CD19. b) Assessment of h1218 binding to CD19 pre-complexed with FMC63. Sensor surfaces were immobilized with FMC63 Fc, followed by CD19-ECD-Ck loading from 1700 to 2300 s. Subsequent addition of FMC63 or h1218 at 2300 s was monitored for incremental binding. c) Evaluation of h1218 binding to wild-type HEK293T cells (CD19-negative), HEK293T expressing full human CD19 (huCD19, HHH), or HEK293T expressing chimeric CD19 variants with cynomolgus substitutions in discrete domains (CHH, HCH, HHC). d) Alanine-scanning mutagenesis to pinpoint residues critical for the h1218 epitope on CD19. e) Measurement of IFNγ secretion triggered by HEK293T cells expressing wild-type or mutated CD19, identifying residues influencing h1218 recognition. f) Kinetic analysis of FMC63 and h1218 scFv binding to recombinant human CD19-ECD-Ck (M1-P278). Curves represent measurements at varying scFv concentrations. Experiments were performed in at least duplicate.

To verify CD19 specificity of the h1218 scFv, we evaluated potential cross-reactivity against a library of 5,484 human plasma membrane or tethered secreted proteins expressed in HEK293 cells (Retrogenix screen). Strong

signal was detected exclusively with CD19, accompanied by weaker, non-specific interactions with TMEM108, SUSD5, and GUCA2A. Functional validation using flow cytometry and ELISA on HEK293T cells overexpressing these candidates demonstrated no activation of h1218-CAR T cells. Thus, off-target binding to TMEM108, SUSD5, or GUCA2A was ruled out.

AT101 (h1218-based CAR T cells) surmount resistance due to loss of the FMC63-binding site on CD19 in experimental models

With a new single-chain variable fragment (scFv) aimed at a membrane-proximal site on CD19 now in hand, we constructed a second-generation chimeric antigen receptor (CAR). We incorporated lentiviral vectors (pTRPE or pLTG) featuring a CD8α hinge and transmembrane segment, paired with 4-1BB co-stimulation and CD3ζ activation domains. Lentiviruses were generated from these vectors to transduce and propagate primary human T lymphocytes using methods outlined previously [20, 28]. The novel therapy (h1218-CART19) was initially evaluated in systems refractory to FMC63-CART19. Clinical samples from individuals relapsing after FMC63-CART19 have revealed two exon 3 mutations in CD19 (R163L and L174V) that abolish the FMC63 binding site and induce resistance [8, 14]. To replicate escape via mutated CD19, we employed CRISPR-Cas9 editing to eliminate native wild-type CD19 from the B-acute lymphoblastic leukemia line Nalm6 (yielding Nalm6-CD19KO), followed by lentiviral delivery of either mutation (producing Nalm6-CD19R163L or Nalm6-CD19L174V) **(Figure 2a).** Flow cytometry validated membrane presentation of these altered CD19 proteins **(Figure 2b).** Short-duration in vitro lysis experiments involving untransduced (UTD) control T cells, FMC63-CART19, or h1218-CART19 showed selective lysis of both Nalm6-CD19R163L and Nalm6-CD19L174V targets exclusively by h1218-CART19 **(Figure 2c).** Supporting this, exposure to either mutant line elicited substantial IL-2 and TNF production from h1218-CART19 but negligible release from FMC63-CART19 ($p < 0.0001$ for each cytokine) **(Figure 2d).** In vivo confirmation focused on the predominant clinical variant, Nalm6-CD19L174V. Immunocompromised NSG mice received 1×10^6 Nalm6-CD19L174V cells on day -5, then—following group allocation—0.75×10^6 UTD, FMC63-CART19, or h1218-CART19 cells on day 0 **(Figure 2e).** Recipients of h1218-CART19 displayed superior leukemia suppression and extended survival (median overall survival: FMC63-CART19 = 9 days versus h1218-CART19 = not reached, $p = 0.0027$) **(Figures 2e and 2f).** Circulating h1218-CART19 expansion also markedly outpaced comparators (mean T cell count: FMC63 = 68 cells/100 µL blood versus h1218 = 300 cells/100 µL blood, $p = 0.0096$) **(Figure 2g).** Taken together, these findings illustrate the capacity of h1218-CART19 to evade resistance arising from disruptions to the FMC63 epitope on CD19.

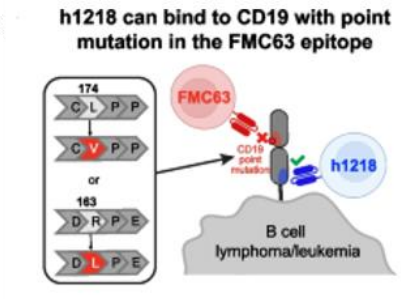

a)

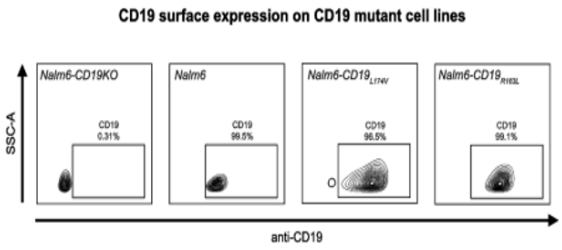

b)

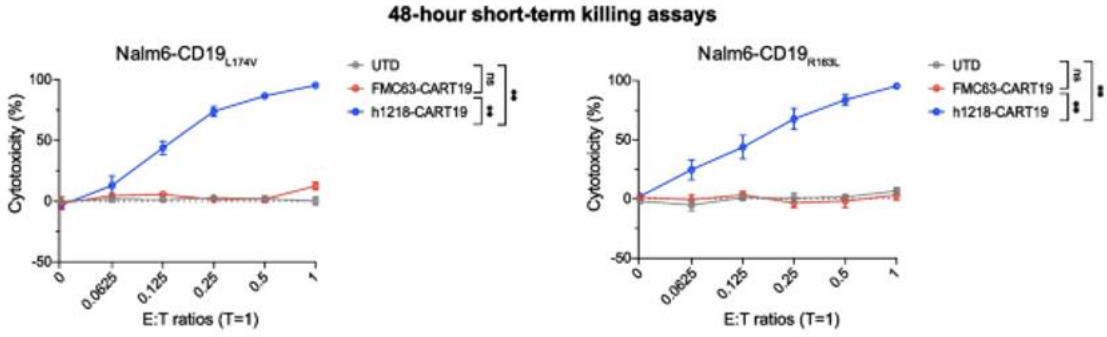

c)

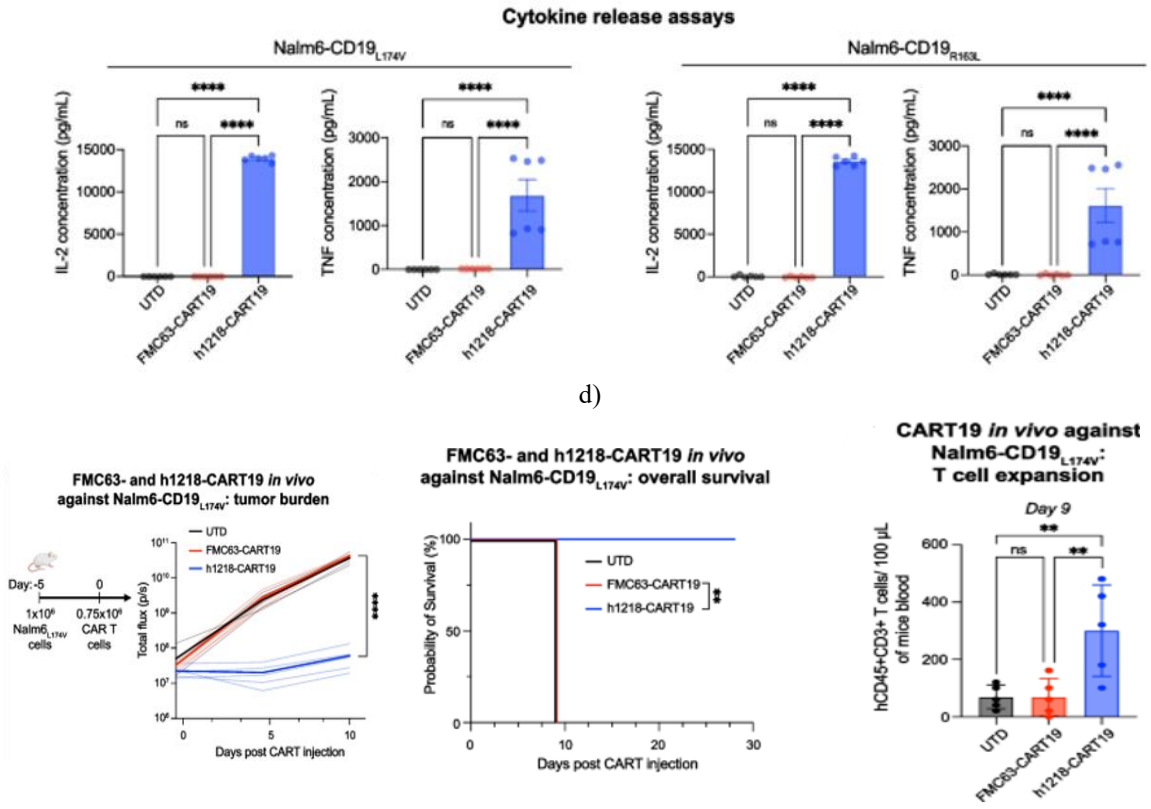

Figure 2. h1218-CART19 detects and destroys leukemic B cells harboring CD19 alterations that confer resistance to FMC63-based therapy. a) Illustration of engineered leukemic B cells bearing documented post-FMC63-CART19 point mutations in the membrane-distal CD19 region (CD19R163L or CD19L174V). b) Flow cytometry determination of CD19 membrane levels on Nalm6-CD19KO, wild-type Nalm6, Nalm6-CD19L174V (left panel), and Nalm6-CD19R163L (right panel) lines. c) Lytic activity of CAR T products toward Nalm6-CD19L174V and Nalm6-CD19R163L across escalating effector-to-target (E:T) ratios (n = 3 separate donors; luciferase readout). d) ELISA assessment of IL-2 and TNF release 24 h post co-incubation of CAR T cells with targets at E:T of 5:1 (n = 2 donors). Readings below the calibration curve are reported as zero. e) (Left) Design of NSG xenograft experiment: intravenous delivery of 1×10^6 luciferase-expressing Nalm6-CD19L174V cells, succeeded 5 days later by 0.75×10^6 UTD, FMC63-CART19, or h1218-CART19 cells. (Right) Leukemia progression tracked via bioluminescence in treated cohorts (UTD n = 5; FMC63-CART19 n = 5; h1218-CART19 n = 5); thick lines denote group medians. f) Survival analysis across arms ($p = 0.0027$). g) Quantification of human CD45+ CD3+ T cells per 100 µL blood on day 9. Data in bars and lysis plots represent mean ± SEM. Kaplan-Meier curves analyzed by log-rank (Mantel-Cox); additional comparisons via one-way ANOVA with Tukey post-test; $p < 0.0001$, * $p < 0.001$, $p < 0.01$, * $p < 0.05$. All bar graphs are presented as mean ± SEM. Replications performed at minimum twice.

h1218-CART19 overcomes a rare mechanism of FMC63 epitope masking in experimental systems

An additional, albeit uncommon, pathway leading to loss of the FMC63-binding site on CD19 involves inadvertent lentiviral transduction of leukemic B cells with the FMC63-CAR19 construct during production, resulting in cis-interaction between the CAR and CD19 that occludes the epitope. Prior work from our group established that such CAR19-positive B-ALL cells acquire resistance to FMC63-CART19 despite persistent surface CD19 display [12]. We hypothesized that h1218-CART19 could engage these targets, as its distinct epitope remains unmasked by the FMC63-CAR19. Accordingly, we generated CD19-positive Nalm6 cells transduced with a lentivirus encoding FMC63-CAR19, yielding dual expression of native CD19 and the FMC63-CAR **(Figures 3a and 3b).** These engineered cells had previously been confirmed as refractory to FMC63-CART19 [12]. In vitro preclinical assays revealed potent short- and long-term killing, along with robust IL-2 release, by h1218-CART19 against Nalm6-FMC63 targets, in stark contrast to the complete lack of response from FMC63-CART19 **(Figures 3c-3e).** To extend these findings in vivo, we evaluated h1218-CART19 activity

against epitope-masked leukemia by injecting NSG mice with 1×10^6 Nalm6-FMC63 cells on day -5, followed by randomization to treatment with 0.75×10^6 untransduced (UTD), FMC63-CART19, or h1218-CART19 cells on day 0 **(Figure 3f).** Strikingly, every mouse receiving h1218-CART19 achieved superior leukemia suppression and markedly prolonged survival compared to the FMC63-CART19 arm (median overall survival: FMC63-CART19 = 7 days versus h1218-CART19 = not reached, p = 0.0016) **(Figures 3f and 3g).** Overall, these data indicate that the innovative h1218-CART19 therapy, directed toward a membrane-proximal CD19 epitope, retains the ability to detect and eliminate relapsed malignant cells exhibiting either CD19 mutations or FMC63 epitope masking following prior CAR T treatment.

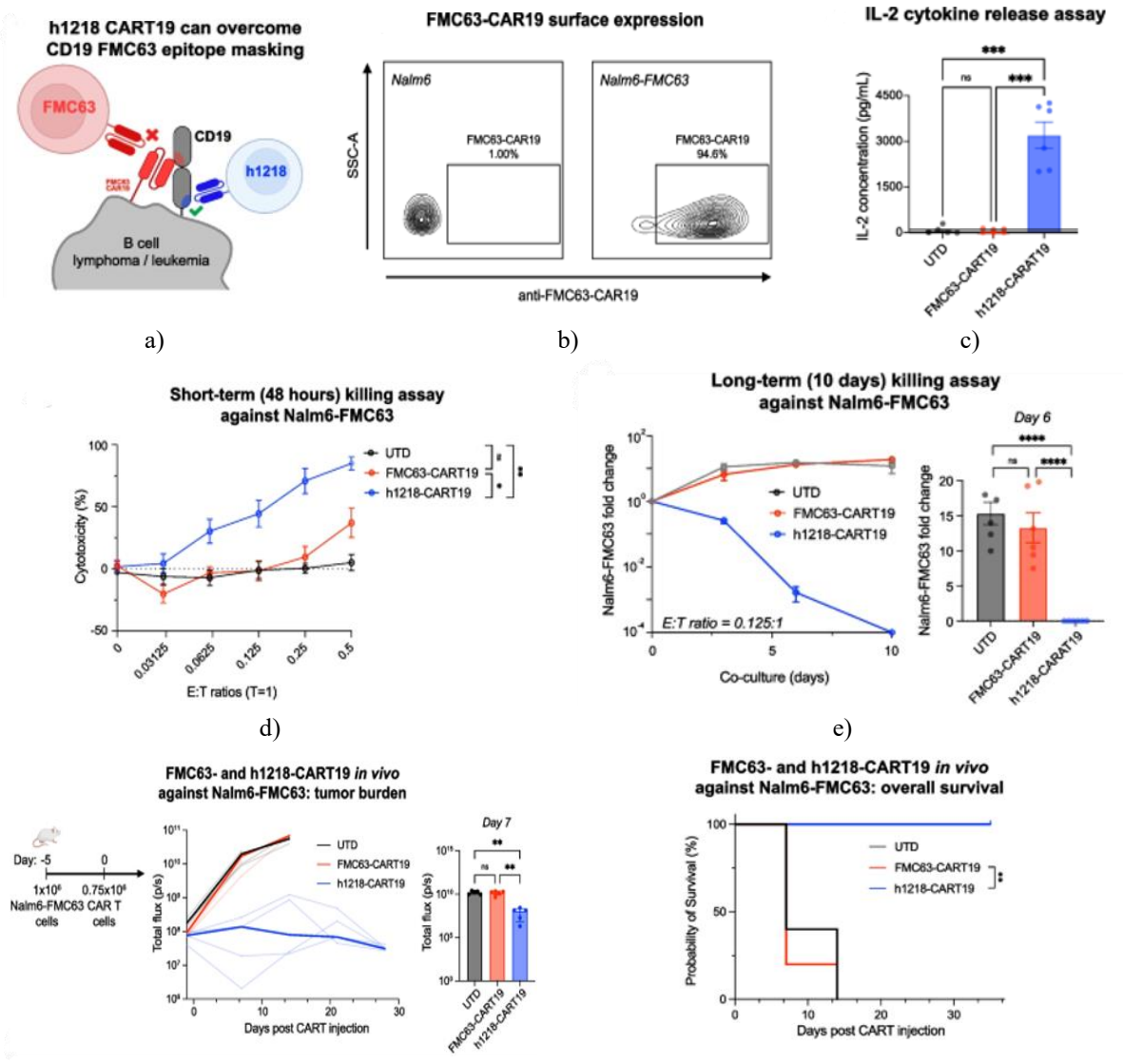

Figure 3. h1218-CART19 effectively targets and eliminates relapsed Nalm6 cells expressing FMC63-CAR19. a) Diagram illustrating accidental incorporation of FMC63-CAR19 lentivirus into a B-cell lymphoma/leukemia cell during manufacturing, causing epitope occlusion and resistance to FMC63-directed CAR T therapy. b) Flow cytometric measurement of FMC63-CAR surface levels on modified Nalm6 cells.c) ELISA-based quantification of IL-2 secretion 24 h after co-culture of CAR T cells with targets at an effector-to-target (E:T) ratio of 5:1 (n = 2 donors). Readings below the standard curve limit are depicted as zero. d) 48-hour cytotoxicity assessment of CAR T products against Nalm6-FMC63 across multiple E:T ratios (n = 2 donors) via flow cytometry. e) Longitudinal monitoring of target cell expansion under CAR T pressure over 10 days (n = 3 donors) by flow cytometry. (Left) Temporal fold change in Nalm6-FMC63 counts relative to day 0. (Right) Fold change in Nalm6-FMC63 on day 6. f) (Left) Outline of the NSG xenograft model: 1×10^6 luciferase-expressing Nalm6-FMC63 cells were administered, followed 5 days later by intravenous delivery

of 0.75 × 10^6 UTD or CAR T cells. (Right) Serial tumor burden assessment in Nalm6-FMC63-bearing mice treated with UTD (n = 5), FMC63-CART19 (n = 5), or h1218-CART19 (n = 5); thick lines indicate group medians. g) Kaplan-Meier overall survival analysis in Nalm6-FMC63-engrafted mice (p = 0.0016). Bar graphs and killing curves display mean ± SEM. Multiple comparisons employed one-way ANOVA with Tukey adjustment; survival differences tested via log-rank (Mantel-Cox); $p < 0.0001$, * $p < 0.001$, $p < 0.01$, * $p < 0.05$. All bar graphs are represented as mean ± SEM. Experiments were conducted in duplicate or more.

h1218-CART19 exhibits superior performance over FMC63-CART19 in preclinical human models of B-cell malignancies

The h1218 scFv, as noted earlier, displays distinct binding kinetics with quicker association and dissociation rates relative to the FMC63 scFv. We proposed that this property might confer advantages to the h1218-based CAR, potentially mitigating activation-induced cell death (AICD) during antigen encounter and yielding better therapeutic outcomes than conventional FMC63-CART19 **(Figure 4a).** To investigate this, we compared the functional profiles of h1218-CART19 and FMC63-CART19 in relevant preclinical settings for non-Hodgkin lymphoma (NHL) and acute lymphoblastic leukemia (ALL), both in vitro and in vivo. Short-duration (48 h) cytotoxicity assays revealed comparable killing efficiency between FMC63-CART19 and h1218-CART19 against Nalm6 and additional hematologic tumor lines **(Figure 4b)**. This equivalence aligned with similar interferon-gamma (IFNγ) secretion profiles from both products when challenged with various B-cell malignancy targets, including Raji (Burkitt lymphoma), Pfeiffer (diffuse large B-cell lymphoma, DLBCL), Toledo (DLBCL), and Nalm6 (B-ALL) **(Figure 4c).** In vivo, h1218-CART19 displayed dose-responsive antitumor effects against Raji cells, and at higher CAR T doses (1.5 × 10^6 cells), both constructs achieved equivalent control of Raji and Nalm6 xenografts **(Figure 4d).**

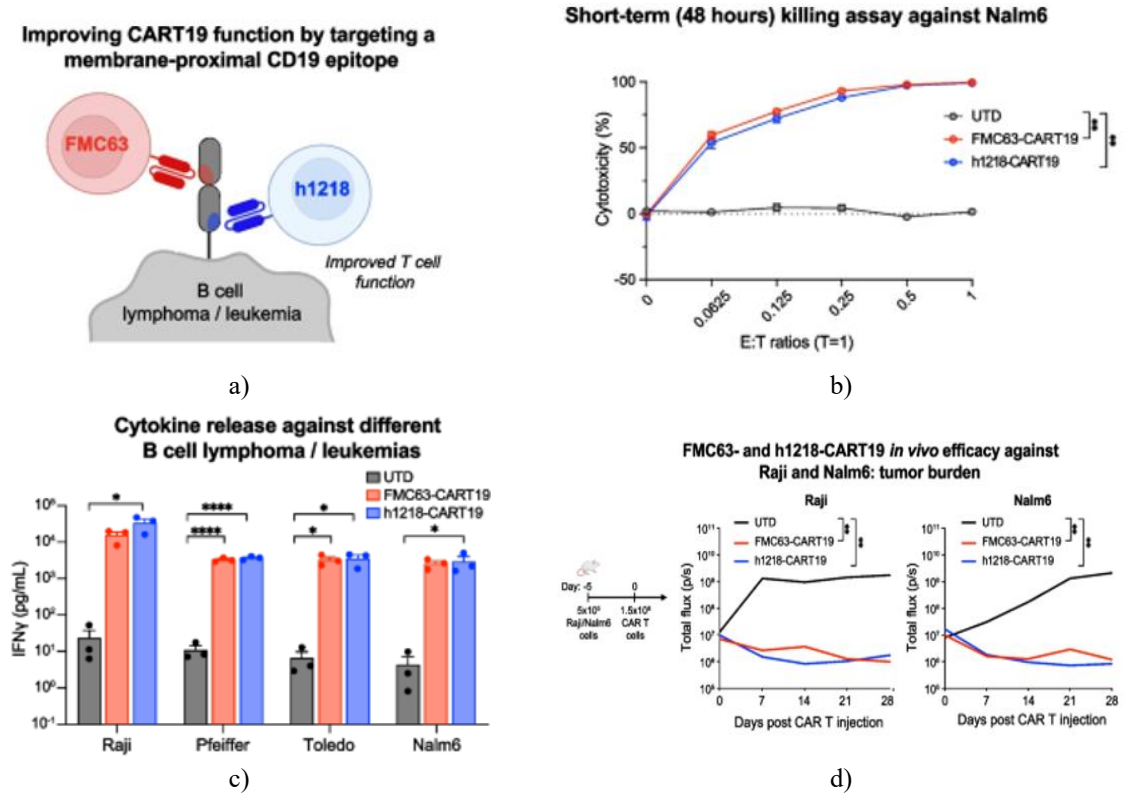

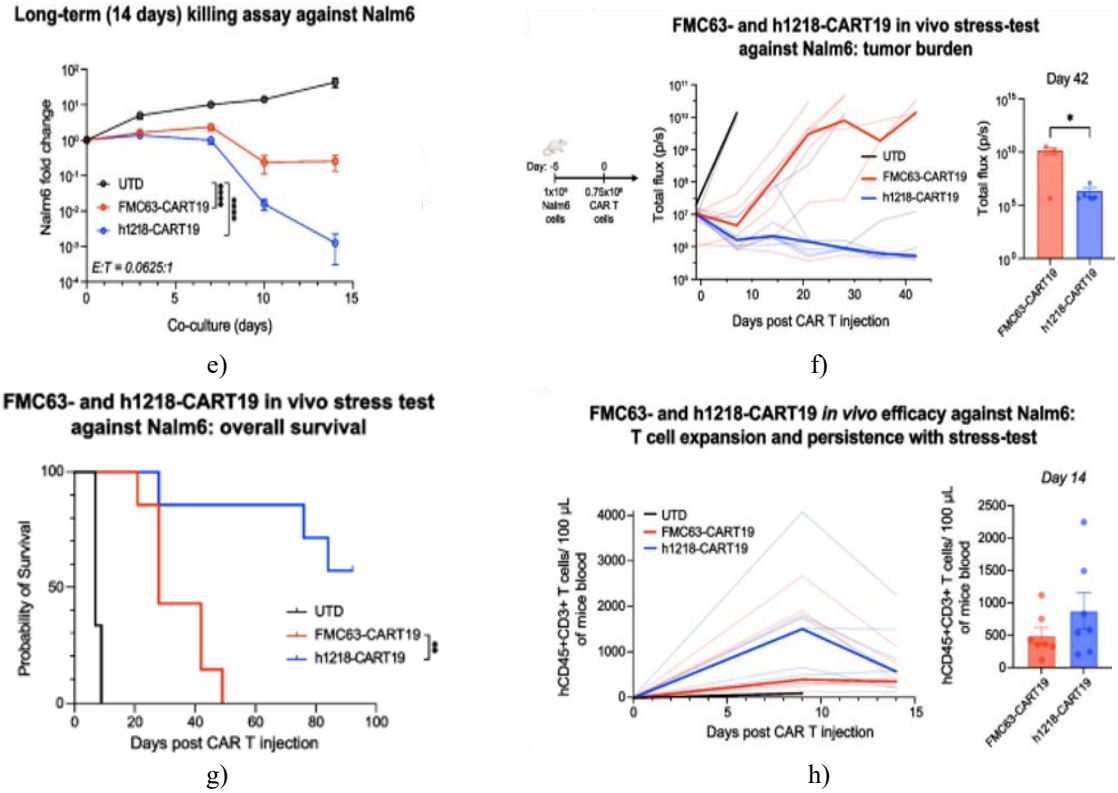

Figure 4. h1218-CART19 outperforms FMC63-CART19 in efficacy. a) Illustration comparing h1218-CART19 binding to the membrane-proximal CD19 region versus the standard FMC63-CART19 targeting site in B-cell lymphoma/leukemia. b) Lysis of Nalm6 targets by untransduced (UTD), h1218-CART19, or FMC63-CART19 cells across multiple effector-to-target (E:T) ratios (n = 3 donors), assessed by flow cytometry. c) ELISA measurement of IFNγ secretion following exposure to CD19-positive tumor lines (Raji, Pfeiffer, Toledo, and Nalm6) at an E:T ratio of 3:1 (n = 2 donors). d) (Left) Design of in vivo study: 1.5×10^6 UTD or CAR T cells administered 7 days post-intravenous inoculation of luciferase-positive Raji or Nalm6 cells. Tumor growth dynamics in Raji-bearing (middle) and Nalm6-bearing (right) mice. e) Long-term monitoring of Nalm6 proliferation over 14 days under low E:T conditions (0.0625:1) with UTD, FMC63-CART19, or h1218-CART19 (n = 2 donors) via flow cytometry. f) (Left) Outline of low-dose xenograft model: 0.75×10^6 UTD or CAR T cells delivered intravenously 5 days after luciferase-positive Nalm6 establishment. (Middle) Longitudinal leukemia burden in Nalm6-engrafted mice receiving UTD (n = 3), FMC63-CART19 (n = 7), or h1218-CART19 (n = 7), tracked by bioluminescence; thick lines denote group medians. (Right) Leukemia signal on day 42 post-CAR T infusion. g) Kaplan-Meier survival analysis for Nalm6-bearing mice. h) (Left) Temporal CAR T cell expansion in peripheral blood following infusion; thick lines indicate medians. (Right) Day 14 CAR T cell counts in blood determined by flow cytometry. Bar graphs and killing curves show mean ± SEM. Two-group comparisons used Student's t-test; multi-group analyses applied one-way ANOVA with Tukey adjustment; survival assessed via log-rank (Mantel-Cox) test; $p < 0.0001$, * $p < 0.001$, $p < 0.01$, * $p < 0.05$. All bar graphs are presented as mean ± SEM. Experiments were replicated at least twice.

In contrast, under challenging "stress-test" conditions employing suboptimal, lower CAR T doses (0.75×10^6 cells), h1218-CART19 consistently outperformed FMC63-CART19 across assays. Specifically, prolonged in vitro co-culture at a very low E:T ratio of 0.0625:1 demonstrated superior suppression of Nalm6 growth by h1218-CART19 relative to FMC63-CART19 **(Figure 4e).** Similarly, in a low-dose Nalm6 NSG xenograft model with 0.75×10^6 CAR-positive T cells, h1218-CART19 achieved markedly improved leukemia containment compared to FMC63-CART19 ($p = 0.042$) **(Figure 4f)**. This translated into substantially extended survival (median overall survival: h1218-CART19 = not reached versus FMC63-CART19 = 28 days, $p = 0.0017$) **(Figure 4g)**. Additionally, monitoring revealed greater in vivo proliferation and sustained presence of h1218-CART19 cells in circulation compared to FMC63-CART19 **(Figure 4h)**. Collectively, these findings highlight the enhanced

preclinical antitumor potency of the innovative h1218-CART19 construct over FMC63-CART19, linked to improved expansion and longevity of the CAR T cells.

Rapid association and dissociation kinetics of h1218-CART19 correlate with reduced activation-induced cell death relative to FMC63-CART19

To elucidate the mechanisms underlying the superior antitumor performance of h1218-CART19 over FMC63-CART19, we investigated CAR T cell–tumor cell interactions. Based on the premise that the quicker on- and off-rates of the h1218 scFv enhance CAR T functionality, we first measured cellular avidity of both products using the z-Movi system (LUMICKS). Consistent with prior scFv kinetic data, h1218-CART19 exhibited lower avidity than FMC63-CART19 (mean avidity: FMC63 = 55.57% versus h1218 = 39.23%, $p < 0.0001$) **(Figure 5a)**. Next, we examined immunological synapse formation as reported previously [29]. Synapse stability was assessed via F-actin accumulation, and physical synapse assembly via CD19 clustering. Reflecting its reduced avidity, h1218-CART19 displayed diminished F-actin polymerization and lower CD19 recruitment at the synapse compared to FMC63-CART19. Early signaling events were evaluated by quantifying polarization of perforin and phosphorylated CD3ζ (pCD3ζ) toward the synapse. At the 2-hour mark post-stimulation, h1218-CART19 showed decreased perforin and pCD3ζ recruitment relative to FMC63-CART19 **(Figures 5b and 5c)**. These observations align with the faster dissociation rate of h1218. Considering the enhanced antitumor activity and in vivo expansion previously noted for h1218-CART19, we posited that its superiority stems from attenuated early activation, lessened AICD, and consequently improved long-term CAR T survival following antigen exposure. To validate this, we quantified AICD after target engagement. Strikingly, h1218-CART19 exhibited lower baseline caspase 3/7 activation and markedly reduced induction of caspase 3/7 cleavage upon stimulation compared to FMC63-CART19 **(Figure 5d)**, indicating elevated AICD in FMC63-CART19 that could diminish sustained T cell populations over time.

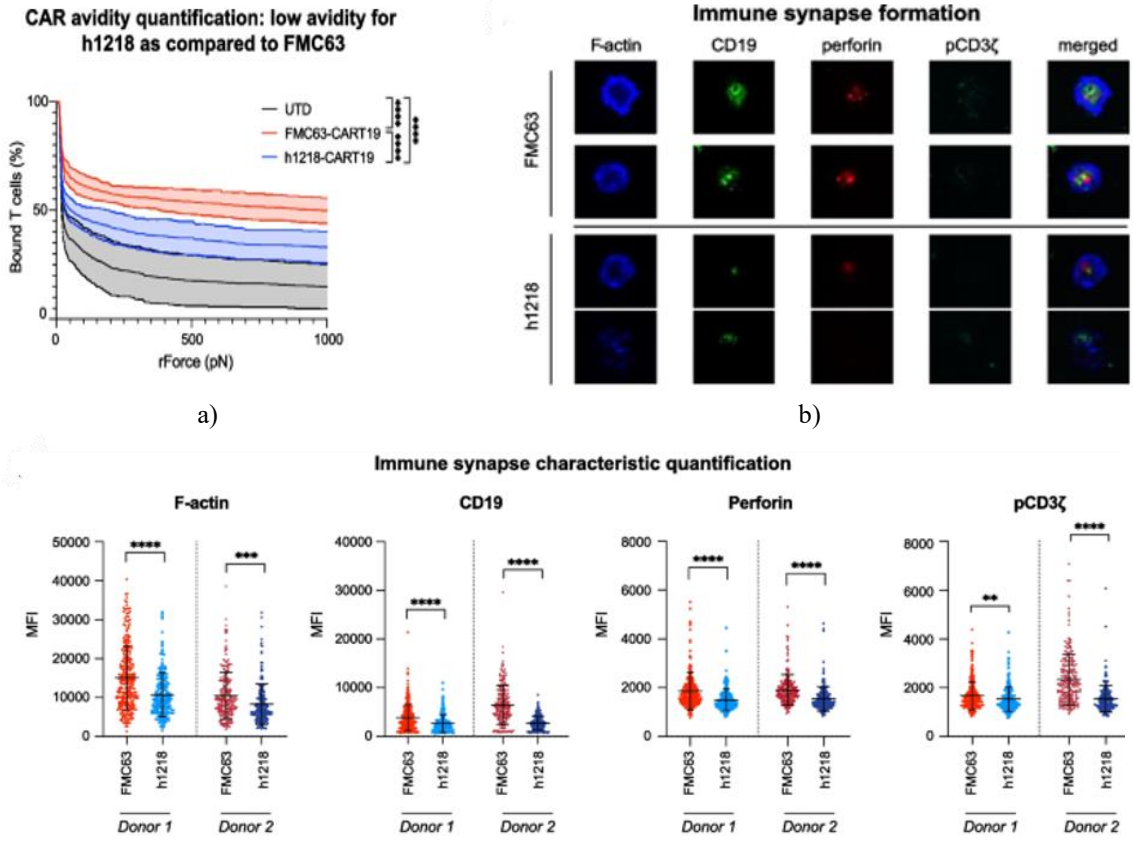

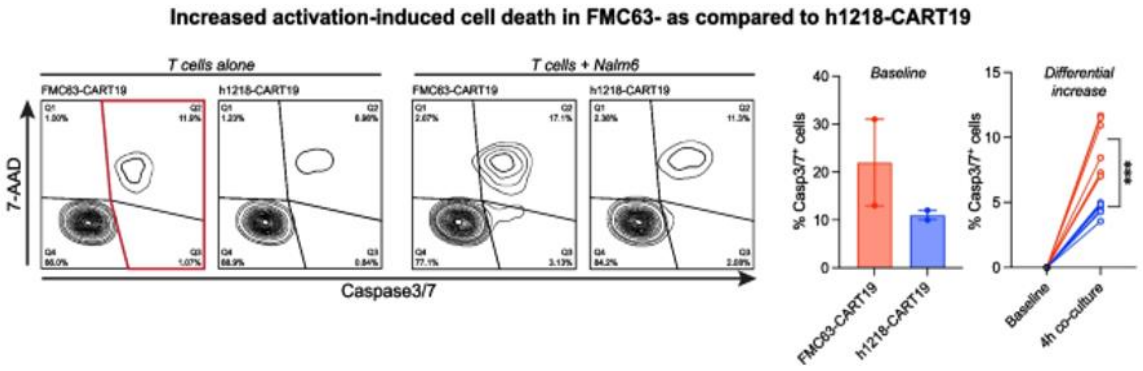

d)

Figure 5. h1218-CART19 displays reduced avidity and diminished activation-induced cell death compared to FMC63-CART19. a) Avidity measurement of untransduced (UTD), FMC63-CART19, and h1218-CART19 cells against Nalm6 targets after 15-minute co-incubation (n = 2 donors) using Lumicks platform. b) Representative confocal images showing F-actin, CD19, perforin, and phosphorylated-CD3ζ (pCD3ζ) (CAR signal) in FMC63-CART19 or h1218-CART19 cells interacting with biotinylated CD19 protein. c) Quantitative analysis of F-actin accumulation, perforin polarization, and pCD3ζ levels in FMC63-CART19 or h1218-CART19 cells upon engagement with biotinylated CD19 (n = 2 donors); 200 synaptic events analyzed per condition. d) (Left) Example flow cytometry plots of Caspase 3/7-positive FMC63-CART19 and h1218-CART19 cells with or without 4-hour Nalm6 stimulation; Caspase 3/7-positive gate highlighted in red. (Middle) Baseline Caspase 3/7-positive fraction in FMC63- or h1218-CART19 at time zero. (Right) Increase in Caspase 3/7-positive cells following 4-hour stimulation. All data presented as mean ± SEM. Two-group comparisons via Student's t-test; multi-group via one-way ANOVA with Tukey adjustment; $p < 0.0001$, * $p < 0.001$, $p < 0.01$, * $p < 0.05$. All bar graphs are presented as mean ± SEM. Experiments replicated at least twice.

First-in-human phase I clinical trial of h1218-CART19 (AT101) in relapsed/refractory non-Hodgkin lymphoma: trial design and participant characteristics

Building on encouraging preclinical data, we advanced the h1218-CART19 construct into a clinical-grade GMP product designated AT101 (AbClon Inc.). A multicenter phase I/II first-in-human study was initiated to determine tolerability and identify the recommended phase II dose (RP2D) of AT101 in adults with B-cell non-Hodgkin lymphoma (NCT05338931). The trial employed a conventional 3 + 3 dose-escalation scheme (detailed in "Methods"). Presented here are preliminary findings from the phase I segment. Major eligibility requirements included confirmed B-NHL refractory or relapsed after ≥1 prior standard regimen, ECOG performance status 0–1, and preserved organ and bone marrow function. Prior exposure to cellular immunotherapy, autologous stem cell transplant (ASCT), or CD3/CD20 bispecific antibodies did not preclude participation. Candidates underwent screening, provided informed consent, and proceeded to enrollment. Autologous T lymphocytes were harvested via routine leukapheresis and processed into AT101 using automated, closed manufacturing platforms. Dose level assignment occurred post-apheresis. Upon product release, participants received lymphodepleting chemotherapy consisting of intravenous fludarabine (25 mg/m²) and cyclophosphamide (250 mg/m²) on days -4, -3, and -2 before infusion. AT101 was delivered as a single intravenous dose at one of three levels: DL-1 (0.2×10^6 cells/kg), DL-2 (1.0×10^6 cells/kg), or DL-3 (5.0×10^6 cells/kg). Bridging therapy was permitted at investigator discretion during manufacturing or until 2 weeks prior to AT101 administration.

As depicted in the CONSORT flowchart, 14 individuals were screened and registered, all of whom advanced to enrollment, resulting in 12 (85.7%) receiving the product infusion. Infusion did not occur in two cases owing to production challenges: poor cellular outgrowth in one instance (n = 1; day 6 expansion fold of 0.70) and microbial contamination of the leukapheresis harvest secondary to subclinical bacteremia, presumably from gut translocation linked to a mucosal abnormality (n = 1). Completed AT101 batches exhibited a median population doubling level of 5.6 (5.2–6.0). The median ratio of CD4 to CD8 subsets was 0.8 (0.1–1.7), while CD45 + CD3 + T lymphocytes comprised 92% (86–95%) of the final composition. Transduction efficiency yielded a median CAR-expressing fraction of 46% (25–57%). The median interval from harvest to product release and infusion was 56

(48–97) days, reflecting the extended durations required for culture-dependent release criteria and quality assurance assays (detailed in Methods).

Clinical profiles for the 12 recipients are compiled in **Table 1**. Median age stood at 62.5 (39–84) years, with women accounting for 58.3% (7/12). Participants had undergone a median of 3 (2–8) prior treatment regimens. Histopathologic distributions were diffuse large B-cell lymphoma (DLBCL, n = 7/12, 58.3%), follicular lymphoma (FL, n = 3/12, 25.0%), mantle cell lymphoma (MCL, n = 1/12, 8.3%), and marginal zone lymphoma (MZL, n = 1/12, 8.3%). ECOG status was 0 for three individuals and 1 for nine. History of autologous stem cell transplant (ASCT) was noted in five (41.7%), prior non-edited NK cell treatment in one (8.3%), and exposure to CD20/CD3 bispecific agents in three (25%). Primary refractory disease characterized two cases (16.7%). Median computed tomography-derived sum of perpendicular lesion diameters (SPD) measured 1,041 (190–11,836) mm^2. Interim systemic treatment bridging apheresis to conditioning was provided to two subjects (16.7%; patients 9 and 12) employing CHOP (cyclophosphamide, doxorubicin, vincristine, prednisone) or ESHAP (etoposide, cisplatin, cytarabine, methylprednisolone) protocols. Bridging yielded no benefit in patient 9 but partial remission in patient 12. Raised lactate dehydrogenase (LDH) occurred in five participants (41.7%). A single case presented bulky (> 7 cm) involvement. Collectively, the population reflected substantial prior therapeutic exposure, encompassing contemporary cellular modalities, albeit without antecedent CD19-directed CAR T administration.

Table 1. Patient baseline characteristics

Patient Characteristic	Value (%)
Age, n (years)	
< 60	5 (41.7)
≥ 60	7 (58.3)
Median (range)	62.5 (39–84)
Lymphoma Histology, n (%)	
Diffuse large B-cell lymphoma (DLBCL)	7 (58.3)
Follicular lymphoma (FL)	3 (25.0)
Mantle cell lymphoma (MCL)	1 (8.3)
Marginal zone lymphoma (MZL)	1 (8.3)
History of prior autologous stem cell transplantation (ASCT), n (%)	5 (41.7)
Number of previous treatment regimens, n (%)	
≤ 2	5 (41.7)
≥ 3	7 (58.3)
Median (range)	3 (2–8)
Refractory disease to last chemotherapy regimen, n (%)	2 (16.7)
Received bridging therapy[a], n (%)	2 (16.7)

Abbreviations: DLBCL diffuse large B cell lymphoma, FL follicular lymphoma, MCL mantle cell lymphoma, MZL marginal zone lymphoma, ASCT autologous stem cell transplantation

^a^Bridging was defined as any therapy received between leukapheresis and the start of LD chemotherapy

Adverse event profile of h1218-CART19 in relapsed/refractory B-cell non-Hodgkin lymphoma

Infusions proceeded without immediate hypersensitivity or acute complications. Grade ≥ 3 toxicities emerged in 58.3% overall **(Table 2).** Neutropenia predominated among serious events, involving seven cases and largely ascribable to the conditioning regimen. Pre-conditioning B-lymphocyte counts below 50 cells/μL were documented in six recipients. Post-treatment B-cell depletion was uniform across the cohort. In patient 8, who manifested progression at month 3, B-cell reconstitution paralleled tumor advancement. Anemia of grade 3 affected four individuals (33.3%), while thrombocytopenia of grade ≥ 3 occurred in two (16.7%). Declines in hemoglobin and platelets were transient post-conditioning, with swift normalization among those achieving response. Ferritin elevations peaked in the first fortnight following administration. Patient 12 encountered grade 3 bacterial sepsis on day 19, resolving under antimicrobials, but later developed fatal candidemia-related septic shock and organ failure after an additional 27 days **(Table 2)**.

Cytokine-release syndrome (CRS) developed in 33.3% (n = 4), attaining grade 3 in one instance (8.3%). No CRS arose at DL-1; grade 1 was seen in three at DL-2/3, with the sole grade 3 case at DL-3. Median CRS initiation

occurred at 6.5 (2–11) days post-administration, subsiding rapidly (within one day). Corticosteroid support was unnecessary for CRS resolution. Neurotoxicity consistent with immune effector cell-associated neurotoxicity syndrome (ICANS) affected 25% (n = 3), including one grade 4 event (8.3%) at DL-1 constituting the trial's only dose-limiting toxicity. This manifested as day 12 encephalopathy requiring ventilatory support for airway security, yet resolved fully sans sequelae after six days of high-dose intravenous dexamethasone combined with intrathecal hydrocortisone. Cohort expansion at DL-1 with three further enrollees yielded no recurrent ICANS. Mild-to-moderate (grade 1–2) neurologic symptoms—tremor in one DL-2 case and delirium in one DL-3 case—comprised the remainder. Median ICANS commencement was day 12 (8–12), achieving full remission within 3 (2–6) days via dexamethasone **(Table 2)**.

Table 2. Summary of adverse events incidence, grade and duration by dose level

Adverse Event	DL-1 (n=6)	DL-2 (n=3)	DL-3 (n=3)	Total (n=12)
Cytokine Release Syndrome (CRS)				
Any grade	0	1	3	4 (33.3)
Grade 1/2	0	1	2	3 (25.0)
Grade ≥3	0	0	1	1 (8.3)
Time to onset, days (range)	-	11	2	6.5 (2–11)
Time from onset to resolution, days (range)	-	1	1	1 (1–1)
Immune Effector Cell-Associated Neurotoxicity Syndrome (ICANS)				
Any grade	1	1	1	3 (25.0)
Grade 1/2	0	1	1	2 (16.7)
Grade ≥3	1	0	0	1 (8.3)
Time to onset, days (range)	12	12	8	12 (8–12)
Time from onset to resolution, days (range)	6	2	3	3 (2–6)
Other Adverse Events				
Patients with any Grade ≥3 adverse event	4	1	2	7 (58.3)
Neutropenia	4	1	2	7 (58.3)
Anemia	3	0	1	4 (33.3)
Thrombocytopenia	1	0	1	2 (16.7)
Infection	1	0	1	2 (16.7)
Anorexia	0	0	1	1 (8.3)
Diarrhea	0	0	1	1 (8.3)
COVID-19	0	1	0	1 (8.3)
Hypokalemia	0	0	1	1 (8.3)
Pneumonia	1	0	0	1 (8.3)
Sepsis	0	0	1	1 (8.3)

Clinical activity of h1218-CART19 in relapsed/refractory B-cell non-Hodgkin lymphoma

Among the 12 treated participants, a single individual (8.3%) failed to achieve response to AT101. The remaining cases yielded an overall response rate (ORR) of 91.7% (95% CI, 56.2–97.0), including complete remission (CR) in 10 patients (75%) **(Figures 6a-6d)**. At the one-month assessment, ORR reached 83.3% (95% CI, 51.6–97.9), with CR documented in 8 patients (66.7%). By month 3, among the 11 surviving patients, all 8 prior responders maintained CR (72.7%; 95% CI, 43.6–92.1). Notably, in the subset receiving higher-dose AT101 (DL-2 and DL-3; n = 6), CR rate was 100% **(Figure 6d)**. Across the cohort, one patient (patient 8) with initial partial response (PR) progressed before month 3; the other 10 responders (10/11) sustained benefit, including one (patient 13) who converted from PR to CR by month 3. With median follow-up of 9.3 months (1.5–16.5 months), progression-free survival (PFS) stood at 75.0% and overall survival (OS) at 82.5%. Neither median PFS nor OS was reached **(Figures 6e and 6f)**. One CR patient (patient 12) succumbed to septic shock. In patients attaining CR, median PFS and OS remained unreached. On the basis of these outcomes, DL-3 was designated the recommended phase II dose.

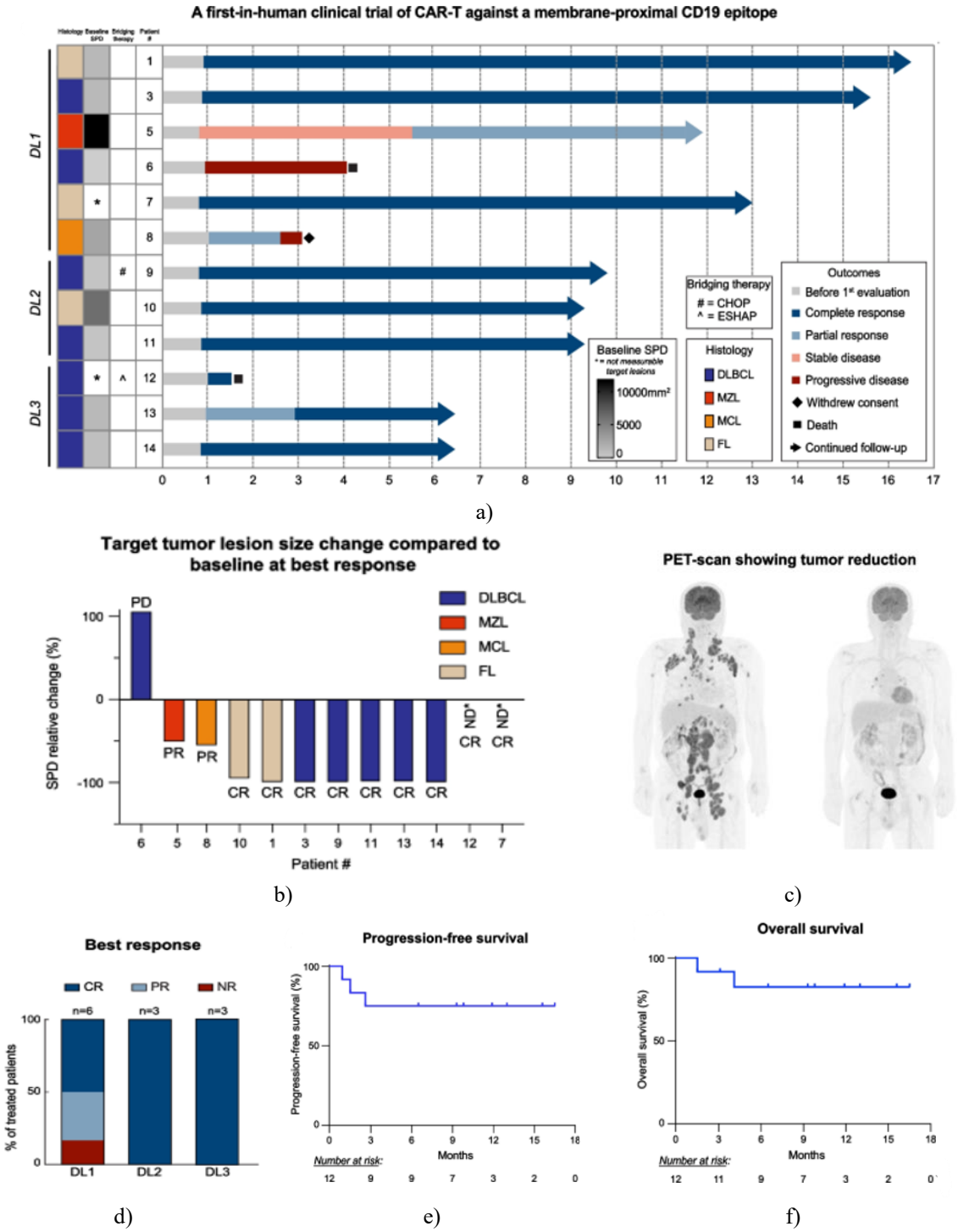

Figure 6. Patient profiles and treatment responses in the h1218-CART19 phase I trial. a) Swimmer plot illustrating individual patient trajectories, response durations, and key features including NHL subtype and baseline tumor burden (sum of product of diameters (SPD), mm²). Refer to legend for details. Note: patient 7 presented non-measurable sigmoid colon involvement at infusion; patient 12 lacked measurable lesions post-bridging. b) Waterfall plot showing maximal tumor reduction from baseline to best post-treatment response per patient. c) Representative PET/CT images from patient 10 pre- and one month post-AT101, demonstrating complete metabolic resolution. d) (Top) Best overall responses in the full cohort of 12 patients. (Bottom) Best responses stratified by dose level (DL-1, DL-2, DL-3). E Progression-free survival among AT101 recipients; patients at risk indicated below. F Overall survival among AT101 recipients; patients at risk indicated below.

Pharmacodynamics of AT101: expansion, persistence, and cytokine profiles

To explore in vivo behavior of AT101 and identify potential biomarkers of efficacy and safety, CAR transgene levels in peripheral blood were quantified by flow cytometry and qPCR, while serum cytokines were assessed via Luminex platform [30]. Peak transgene detection occurred at median day 11 (11–14) post-infusion. Expansion magnitude correlated with administered dose (DL-1: 2.5 ± 1.3; DL-2: 5.0 ± 3.4; DL-3: 113.6 ± 6.50 × 10^4 CAR copies/µg DNA) **(Figure 7a).** Post-infusion serum analysis revealed elevations in multiple inflammatory mediators, most prominently sFas ligand, granzyme A, and perforin, with peaks aligning at day 11 **(Figure 7b)**.

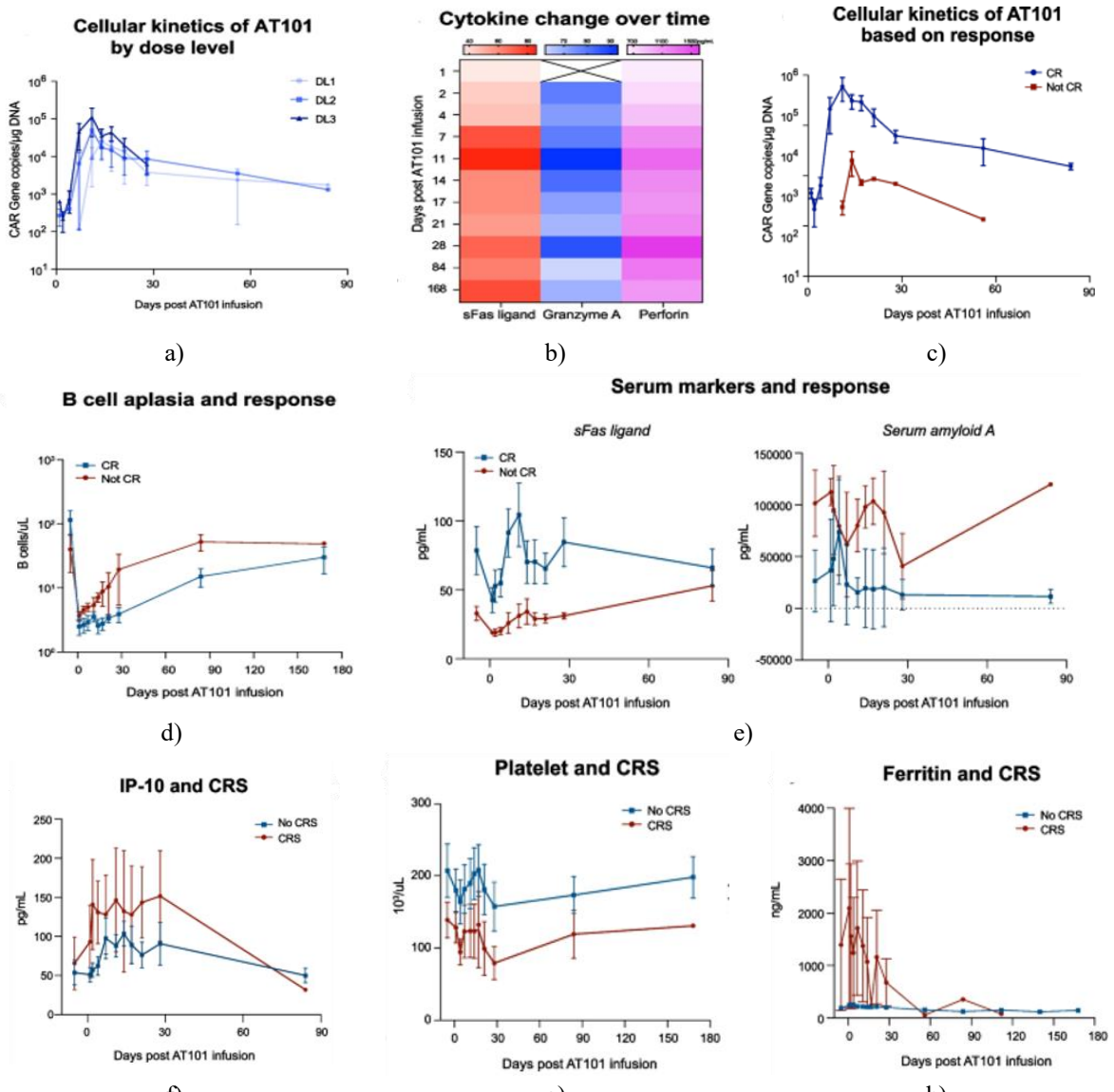

Figure 7. CAR T dynamics, hematologic parameters, and cytokine patterns in the h1218-CART19 phase I study. a) AT101 transgene kinetics and persistence in blood by qPCR across DL-1, DL-2, and DL-3. b)Temporal mean serum concentrations of sFas ligand, granzyme A, and perforin in the 12-patient cohort via Luminex. c) Peak AT101 expansion in patients achieving CR (n = 9) versus non-CR (n = 3) by qPCR. d) Peripheral B-cell counts in CR (n = 9) versus non-CR (n = 3) patients. e) (Left) sFas ligand and (right) serum amyloid A trajectories from day 1 pre-infusion through days 2–168 post-infusion in CR versus non-CR groups via Luminex. f) IP-10 serum dynamics in patients without CRS (n = 8) versus with CRS (n = 4) via Luminex. g) Platelet trends in patients without CRS (n = 8) versus with CRS (n = 4). h) Ferritin kinetics in patients without CRS (n = 8) versus with CRS (n = 4).

Comparative analysis revealed higher peak transgene burdens in CR achievers (6.0×10^4 copies/μg DNA) than in non-CR cases (2.0×10^4 copies/μg DNA) (**Figure 7c).** Sustained B-cell suppression during follow-up similarly tracked with CR status **(Figure 7d).** Elevated sFas ligand distinguished CR patients, whereas serum amyloid A rose preferentially in non-CR individuals **(Figure 7e).** CRS-associated cases exhibited heightened cytokine release, notably IP-10 **(Figure 7f),** alongside more pronounced platelet declines **(Figure 7g)** and greater ferritin excursions **(Figure 7h).**

In conclusion, we successfully translated a novel CD19-targeted CAR T construct from preclinical development to clinical application, demonstrating that a fast-kinetic, membrane-proximal epitope-directed CAR confers robust antitumor efficacy alongside a tolerable safety profile in this patient population.

CD19-directed CAR T cell therapies have delivered impressive clinical outcomes in B-cell malignancies [13, 31, 32]. Regrettably, most recipients of currently approved CAR T products either fail to respond initially or ultimately experience relapse [33]. The primary aim of this work was to engineer and evaluate clinically a next-generation CAR T construct targeting a distinct, non-FMC63 CD19 epitope with rapid association and dissociation kinetics, seeking superior efficacy and resistance profiles that do not overlap with existing therapies. By screening a chicken-derived library against the human CD19 extracellular domain, we isolated a unique anti-CD19 scFv (h1218) that binds a membrane-proximal epitope with characteristically lower avidity. The resulting product, AT101, exhibited a favorable safety profile and achieved a 100% response rate at the selected recommended phase II dose.

All four FDA-approved CD19 CAR T therapies employ the identical FMC63-derived scFv and engage the same antigenic site. Nevertheless, malignant cells can acquire escape mechanisms under selective pressure, culminating in relapse [8, 12, 14, 34, 35]. Notably, absence or reduced expression of the targeted CD19 epitope compromises CAR T effector function in vitro and in vivo while also curtailing long-term in vivo persistence [36]. Earlier reports have pinpointed mutations in CD19 exons 2–5 as predominant drivers of antigen loss [14]. Here, we concentrated on FMC63 epitope disruption via point mutations in CD19 or epitope occlusion through cis CAR19:CD19 interactions. Our preclinical data established superior antitumor potency of h1218-CART19 relative to standard constructs across leukemia and lymphoma models. Specifically, only h1218-CART19—but not FMC63-CART19—effectively detected and eradicated engineered cell lines recapitulating clinical relapse scenarios with FMC63 resistance.

Beyond antigen escape, T cell exhaustion impairs CAR T survival and cytotoxicity within the hostile tumor milieu [37]. We posited that refining CAR–antigen engagement dynamics would bolster in vivo persistence and antitumor performance. Prior investigations indicate that reduced-affinity CARs, particularly under low antigen density, mitigate over-stimulation, limit activation and exhaustion, and foster sustained responses [11, 38- 40], an effect attributed largely to accelerated dissociation rates. For h1218, we anticipated enhanced serial target elimination—critical for durable control [19]. Thus, alongside novel epitope specificity, a CAR retaining comparable equilibrium affinity to FMC63 but featuring accelerated on- and off-rates was expected to augment serial killing while diminishing activation-induced cell death (AICD) and improving overall efficacy. CAR T cells are vulnerable to Fas/DR5-mediated fratricidal AICD upon exceeding activation thresholds, compromising potency [41]. Strategies incorporating dominant-negative Fas receptors to block Fas–FasL signaling have enhanced activity and persistence [42], though often at the cost of heightened inflammatory cytokines and toxicity risk [43]. In contrast, h1218-CART19 displayed attenuated early activation upon CD19 encounter, coupled with superior in vivo expansion and leukemia control versus FMC63-CART19 in xenografts. These findings concord with reports of distinct early activation transcriptomes and phenotypes in rapid-off-rate CARs [39] and, crucially, occurred without exaggerated cytokine release or systemic toxicity. Thus, even at equivalent affinity, elevating dissociation rate yields functional gains, positioning h1218-CART19 to address both FMC63 epitope loss and enhanced baseline activity through reduced AICD.

Guided by these preclinical observations, we launched a multicenter, first-in-human phase I study assessing safety and feasibility of AT101 in relapsed/refractory non-Hodgkin lymphoma. Twelve patients received escalating doses following lymphodepletion. At therapeutically active levels (DL-2 and DL-3), both overall and complete response rates reached 100%. Adverse events remained controllable: severe CRS occurred in only one of six higher-dose recipients, with no severe ICANS at these levels. Neurotoxicity timing appeared somewhat delayed relative to approved products, potentially reflecting AT101 kinetic properties, albeit sample size precludes firm conclusions. AT101 proved active across diverse NHL histologies, notably DLBCL and follicular lymphoma. In these prevalent subtypes, early outcomes compare encouragingly with published rates for axicabtagene ciloleucel,

lisocabtagene maraleucel, and tisagenlecleucel [33, 44], notwithstanding the limited cohort size. Robust in vivo expansion and persistence corroborated preclinical evidence that lower avidity shields against AICD, supporting progressive proliferation beyond 30 days and prolonged durability. Universal post-infusion elevations of effector molecules—chiefly sFas ligand, granzyme A, and perforin—were observed, whereas classical proinflammatory cytokines (IL-6, IL-1, GM-CSF, TNF, IFNγ) showed no marked surges, even in toxicity cases. This distinct cytokine signature implies that low-avidity, rapid-kinetic, alternate-epitope targeting uniquely modulates CAR T behavior.

The patient population receiving AT101 had undergone extensive prior therapies, encompassing anti-CD19 antibodies, bispecific antibodies, and investigational NK cell treatments. Nonetheless, none of the individuals achieving complete remission (CR) has experienced relapse thus far, albeit with limited follow-up duration. While preclinical investigations indicate that AT101 can circumvent certain FMC63-associated resistance pathways, including CD19 epitope disruption, this capability requires confirmation in dedicated prospective clinical studies. Encouragingly, no instances of CD19-negative relapse have emerged among AT101-treated patients to date. This investigation carries inherent constraints typical of initial human trials, including the small patient cohort and clinical heterogeneity. Additionally, the median vein-to-vein interval was prolonged relative to select commercially available CART19 therapies. Although turnaround times of 1–2 months are not unusual in real-world commercial applications, we anticipate abbreviated release testing in upcoming phase II studies, thereby shortening patient wait periods. With the recommended phase II dose now established, the expansion phase II component will evaluate AT101 efficacy specifically in relapsed/refractory diffuse large B-cell lymphoma (DLBCL).

Conclusion

In conclusion, we engineered a CAR antigen-binding domain capable of engaging a distinct membrane-proximal CD19 epitope with accelerated association and dissociation kinetics. These properties conferred superior preclinical performance over FMC63-derived CART19, attributable to alternate epitope targeting, diminished activation-induced cell death (AICD), and tempered activation dynamics. These observations were successfully advanced into a first-in-human trial demonstrating substantial clinical activity—achieving 100% complete remission at dose levels 2 and 3—accompanied by a tolerable safety profile.

Acknowledgments: None

Conflict of Interest: None

Financial Support: None

Ethics Statement: None

References

1. Schuster SJ, Tam CS, Borchmann P, Worel N, McGuirk JP, Holte H, Waller EK, Jaglowski S, Bishop MR, Damon LE, et al. Long-term clinical outcomes of tisagenlecleucel in patients with relapsed or refractory aggressive B-cell lymphomas (JULIET): a multicentre, open-label, single-arm, phase 2 study. Lancet Oncol. 2021;22:1403–15.
2. Lu J, Jiang G. The journey of CAR-T therapy in hematological malignancies. Mol Cancer. 2022;21:194.
3. Vairy S, Garcia JL, Teira P, Bittencourt H. CTL019 (tisagenlecleucel): CAR-T therapy for relapsed and refractory B-cell acute lymphoblastic leukemia. Drug Des Devel Ther. 2018;12:3885–98.
4. Roberts ZJ, Better M, Bot A, Roberts MR, Ribas A. Axicabtagene ciloleucel, a first-in-class CAR T cell therapy for aggressive NHL. Leuk Lymphoma. 2018;59:1785–96.
5. Mao R, Kong W, He Y. The affinity of antigen-binding domain on the antitumor efficacy of CAR T cells: moderate is better. Front Immunol. 2022;13:1032403.
6. Ruella M, Maus MV. Catch me if you can: leukemia escape after CD19-directed T cell immunotherapies. Comput Struct Biotechnol J. 2016;14:357–62.

7. Qin H, Dong Z, Wang X, Cheng WA, Wen F, Xue W, Sun H, Walter M, Wei G, Smith DL, et al. CAR T cells targeting BAFF-R can overcome CD19 antigen loss in B cell malignancies. Sci Transl Med. 2019;11:eaaw9414.
8. Sotillo E, Barrett DM, Black KL, Bagashev A, Oldridge D, Wu G, Sussman R, Lanauze C, Ruella M, Gazzara MR, et al. Convergence of acquired mutations and alternative splicing of CD19 enables resistance to CART-19 immunotherapy. Cancer Discov. 2015;5:1282–95.
9. Duan Y, Chen R, Huang Y, Meng X, Chen J, Liao C, Tang Y, Zhou C, Gao X, Sun J. Tuning the ignition of CAR: optimizing the affinity of scFv to improve CAR-T therapy. Cell Mol Life Sci. 2021;79:14.
10. Ghorashian S, Kramer AM, Onuoha S, Wright G, Bartram J, Richardson R, Albon SJ, Casanovas-Company J, Castro F, Popova B, et al. Enhanced CAR T cell expansion and prolonged persistence in pediatric patients with ALL treated with a low-affinity CD19 CAR. Nat Med. 2019;25:1408–14.
11. Michelozzi IM, Gomez-Castaneda E, Pohle RVC, Cardoso Rodriguez F, Sufi J, Puigdevall Costa P, Subramaniyam M, Kirtsios E, Eddaoudi A, Wu SW, et al. Activation priming and cytokine polyfunctionality modulate the enhanced functionality of low-affinity CD19 CAR T cells. Blood Adv. 2023;7:1725–38.
12. Ruella M, Xu J, Barrett DM, Fraietta JA, Reich TJ, Ambrose DE, Klichinsky M, Shestova O, Patel PR, Kulikovskaya I, et al. Induction of resistance to chimeric antigen receptor T cell therapy by transduction of a single leukemic B cell. Nat Med. 2018;24:1499–503.
13. Ruella M, Gill S. How to train your T cell: genetically engineered chimeric antigen receptor T cells versus bispecific T-cell engagers to target CD19 in B acute lymphoblastic leukemia. Expert Opin Biol Ther. 2015;15:761–6.
14. Zhang Z, Chen X, Tian Y, Li F, Zhao X, Liu J, Yao C, Zhang Y. Point mutation in CD19 facilitates immune escape of B cell lymphoma from CAR-T cell therapy. J Immunother Cancer. 2020;8:e001150.
15. Kouro T, Himuro H, Sasada T. Exhaustion of CAR T cells: potential causes and solutions. J Transl Med. 2022;20:239.
16. Haso W, Lee DW, Shah NN, Stetler-Stevenson M, Yuan CM, Pastan IH, Dimitrov DS, Morgan RA, FitzGerald DJ, Barrett DM, et al. Anti-CD22-chimeric antigen receptors targeting B-cell precursor acute lymphoblastic leukemia. Blood. 2013;121:1165–74.
17. James SE, Greenberg PD, Jensen MC, Lin Y, Wang J, Till BG, Raubitschek AA, Forman SJ, Press OW. Antigen sensitivity of CD22-specific chimeric TCR is modulated by target epitope distance from the cell membrane. J Immunol. 2008;180:7028–38.
18. Singh N, Frey NV, Engels B, Barrett DM, Shestova O, Ravikumar P, Cummins KD, Lee YG, Pajarillo R, Chun I, et al. Antigen-independent activation enhances the efficacy of 4–1BB-costimulated CD22 CAR T cells. Nat Med. 2021;27:842–50.
19. Roddie C, Dias J, O'Reilly MA, Abbasian M, Cadinanos-Garai A, Vispute K, Bosshard-Carter L, Mitsikakou M, Mehra V, Roddy H, et al. Durable responses and low toxicity after fast off-rate CD19 chimeric antigen receptor-T therapy in adults with relapsed or refractory B-cell acute lymphoblastic leukemia. J Clin Oncol. 2021;39:3352–63.
20. Milone MC, Fish JD, Carpenito C, Carroll RG, Binder GK, Teachey D, Samanta M, Lakhal M, Gloss B, Danet-Desnoyers G, et al. Chimeric receptors containing CD137 signal transduction domains mediate enhanced survival of T cells and increased antileukemic efficacy in vivo. Mol Ther. 2009;17:1453–64.
21. Lee YG, Guruprasad P, Ghilardi G, Pajarillo R, Sauter CT, Patel R, Ballard HJ, Hong SJ, Chun I, Yang N, et al. Modulation of BCL-2 in both T Cells and Tumor Cells to Enhance Chimeric Antigen Receptor T cell Immunotherapy against Cancer. Cancer Discov. 2022;12:2372.
22. Liu D, Bryceson YT, Meckel T, Vasiliver-Shamis G, Dustin ML, Long EO. Integrin-dependent organization and bidirectional vesicular traffic at cytotoxic immune synapses. Immunity. 2009;31:99–109.
23. Liu D, Peterson ME, Long EO. The adaptor protein Crk controls activation and inhibition of natural killer cells. Immunity. 2012;36:600–11.
24. Schuster SJ, Svoboda J, Chong EA, Nasta SD, Mato AR, Anak O, Brogdon JL, Pruteanu-Malinici I, Bhoj V, Landsburg D, et al. Chimeric Antigen Receptor T Cells in Refractory B-Cell Lymphomas. N Engl J Med. 2017;377:2545.
25. Lee DW, Santomasso BD, Locke FL, Ghobadi A, Turtle CJ, Brudno JN, Maus MV, Park JH, Mead E, Pavletic S, et al. ASTCT consensus grading for cytokine release syndrome and neurologic toxicity associated with immune effector cells. Biol Blood Marrow Transplant. 2019;25:625–38.

26. Cheson BD, Fisher RI, Barrington SF, Cavalli F, Schwartz LH, Zucca E, Lister TA, Alliance AL, Lymphoma G, Eastern Cooperative Oncology G, et al. Recommendations for initial evaluation, staging, and response assessment of Hodgkin and non-Hodgkin lymphoma: the Lugano classification. J Clin Oncol. 2014;32:3059–68.
27. Sommermeyer D, Hill T, Shamah SM, Salter AI, Chen Y, Mohler KM, Riddell SR. Fully human CD19-specific chimeric antigen receptors for T-cell therapy. Leukemia. 2017;31:2191–9.
28. Lee YG, Guruprasad P, Ghilardi G, Pajarillo R, Sauter CT, Patel R, Ballard HJ, Hong SJ, Chun I, Yang N, et al. Modulation of BCL-2 in both T cells and tumor cells to enhance chimeric antigen receptor T-cell immunotherapy against cancer. Cancer Discov. 2022;12:2372–91.
29. Xiong W, Chen Y, Kang X, Chen Z, Zheng P, Hsu YH, Jang JH, Qin L, Liu H, Dotti G, Liu D. Immunological synapse predicts effectiveness of chimeric antigen receptor cells. Mol Ther. 2018;26:963–75.
30. Kalos M, Levine BL, Porter DL, Katz S, Grupp SA, Bagg A, June CH. T cells with chimeric antigen receptors have potent antitumor effects and can establish memory in patients with advanced leukemia. Sci Transl Med. 2011;3:95ra73.
31. Kochenderfer JN, Dudley ME, Kassim SH, Somerville RP, Carpenter RO, Stetler-Stevenson M, Yang JC, Phan GQ, Hughes MS, Sherry RM, et al. Chemotherapy-refractory diffuse large B-cell lymphoma and indolent B-cell malignancies can be effectively treated with autologous T cells expressing an anti-CD19 chimeric antigen receptor. J Clin Oncol. 2015;33:540–9.
32. Ying Z, Huang XF, Xiang X, Liu Y, Kang X, Song Y, Guo X, Liu H, Ding N, Zhang T, et al. A safe and potent anti-CD19 CAR T cell therapy. Nat Med. 2019;25:947–53.
33. Ghilardi G, Braendstrup P, Chong EA, Schuster SJ, Svoboda J, Ruella M. CAR-T TREK through the lymphoma universe, to boldly go where no other therapy has gone before. Br J Haematol. 2021;193(3):449–65.
34. Chu SH, Small D. Mechanisms of resistance to FLT3 inhibitors. Drug Resist Updat. 2009;12:8–16.
35. Mullighan CG, Phillips LA, Su X, Ma J, Miller CB, Shurtleff SA, Downing JR. Genomic analysis of the clonal origins of relapsed acute lymphoblastic leukemia. Science. 2008;322:1377–80.
36. Ramakrishna S, Highfill SL, Walsh Z, Nguyen SM, Lei H, Shern JF, Qin H, Kraft IL, Stetler-Stevenson M, Yuan CM, et al. Modulation of target antigen density improves CAR T-cell functionality and persistence. Clin Cancer Res. 2019;25:5329–41.
37. Cerrano M, Ruella M, Perales MA, Vitale C, Faraci DG, Giaccone L, Coscia M, Maloy M, Sanchez-Escamilla M, Elsabah H, et al. The advent of CAR T-cell therapy for lymphoproliferative neoplasms: integrating research into clinical practice. Front Immunol. 2020;11:888.
38. Caraballo Galva LD, Jiang X, Hussein MS, Zhang H, Mao R, Brody P, Peng Y, He AR, Kehinde-Ige M, Sadek R, et al. Novel low-avidity glypican-3 specific CARTs resist exhaustion and mediate durable antitumor effects against HCC. Hepatology. 2022;76:330–44.
39. Michelozzi IM, Gomez-Castaneda E, Pohle RVC, Cardoso Rodriguez F, Sufi J, Puigdevall-Costa P, et al. Activation priming and cytokine polyfunctionality modulate the enhanced functionality of low-affinity CD19 CAR T cells. Blood Adv. 2023;7(9):1725–38.
40. Hoseini SS, Dobrenkov K, Pankov D, Xu XL, Cheung NK. Bispecific antibody does not induce T-cell death mediated by chimeric antigen receptor against disialoganglioside GD2. Oncoimmunology. 2017;6:e1320625.
41. Kunkele A, Johnson AJ, Rolczynski LS, Chang CA, Hoglund V, Kelly-Spratt KS, Jensen MC. Functional tuning of CARs reveals signaling threshold above which $CD8^+$ CTL antitumor potency is attenuated due to cell Fas-FasL-dependent AICD. Cancer Immunol Res. 2015;3:368–79.
42. Yamamoto TN, Lee PH, Vodnala SK, Gurusamy D, Kishton RJ, Yu Z, Eidizadeh A, Eil R, Fioravanti J, Gattinoni L, et al. T cells genetically engineered to overcome death signaling enhance adoptive cancer immunotherapy. J Clin Invest. 2019;129:1551–65.
43. Cox MJ, Manriquez Roman C, Tapper EE, Siegler EL, Chappell D, Durrant C, Ahmed O, Sinha S, Mwangi R, Scott NS, et al. GM-CSF disruption in CART cells modulates T cell activation and enhances CART cell anti-tumor activity. Leukemia. 2022;36:1635–45.
44. Sureda A, Lugtenburg PJ, Kersten MJ, Subklewe M, Spanjaart A, Shah NN, et al. Cellular therapy in lymphoma. Hematol Oncol. 2023. https://doi.org/10.1002/hon.3200.